# Paleoenvironmental reconstruction of the cold mid-Paleocene

Comparing the New Jersey shelf and the North Sea basin

Msc. thesis
Suning Hou 5891531

Supervisors:

Dr. Peter k. Bijl

Prof. dr. Appy Sluijs

Utrecht University

## Abstract

Mid-Paleocene (62-58Ma) is a relatively cool period which was scarcely studied. Paleoclimate reconstructions of the relatively cool period mid-Paleocene can provide a better insight of the transition from green house towards Eocene hothouse. Due to the low sea level, sedimentary archives that capture this time interval are scarce. This study provides a complete biostratigraphy framework and $\delta^{13}C_{org}$ sequence of the Paleocene in the North Sea basin core 22/10a-5, and also investigated the paleoenvironmental change dinocysts assemblages. Results from the North Sea Basin core were compared with new analyses on sediments from the Eastcoast US (New Jersey shelf Bass River Core) for New Jersey shelf ODP 174AX which has been intensively studied for the PETM. The integration of $TEX_{86}$-based SST reconstructions from Bass River with existing records in other regions imply that there is a highly reduced meridional temperature gradient occurred in the southern hemisphere while the gradient in the northern hemisphere was large. This is very likely due to the presence of ice sheet in the southern hemisphere. Palynological study revealed that sea level changed synchronously in both sites and low marine paleo-productivity during cold low sea level period. However, productivity would increase in the climate warming stage as a consequence of intensified precipitation and terrestrial input. Latest Danian event (LDE) and North Atlantic Igneous Province (NAIP) were also reflected in the North Sea section.

# Contents

**1.Introduction**

Considering the unabated $CO_2$ emissions by humans, the warm climate in Eocene and its analogously high $CO_2$ concentrations (Beerling and Royer, 2011) has been presented as an analogue to the future of human's era in which all the reserved fossil fuels are combusted. As such, the Eocene climate has attained much attnetion in paleoclimate research, but many questions remain on the nature and development of the Eocene greenhouse climates. The mid-Paleocene preceding Eocene represents a relatively cool phase amidst relatively warm early Paleocene and very warm early Eocene climates (Zachos et al., 2001). The mid-Paleocene represents the onset of the transition towards Eocene hothouse conditions but is a scarcely studied time interval. Even though the information on mid-Paleocene is limited, the available records suggest low ocean surface and deep temperatures (Bijl et al., 2009; Westerhold et al., 2011; Contreras et al., 2014; Hollis et al., 2014), low $CO_2$ concentrations (Beerling and Royer, 2011) and low sea level (Gausti et al., 2005). Southern high-latitude sea-surface temperatures in the mid-Paleocene were at least regionally as cold as when the first major ice sheets of the Cenozoic appeared around 34 Ma (Zachos et al., 2008) (Figure 1). The low sea level in the mid-Paleocene, particularly when considering the time scales at hand (Miller et al., 2005) would invite the idea of the presence of continental ice sheets. However, there is no physical evidence for ice on Antarctica, nor do high-resolution deep-sea benthic foraminiferal oxygen isotope show any orbital forcing in the obliquity band showing that ice sheet dynamics did not imprint the isotope signal (Westerhold et al., 2011). As yet, the presence of ice sheets remains elusive.

The PETM warming has been presented as best analogue to future climate change when all fossil fuels are to be combusted. However, warming of the PETM started from an ice-free climatic state, while our Earth today does contain polar ice sheets. In this case, the mid-Paleocene warming represents an analogue to future climate change which starts from colder background conditions to understand the consequences of climatic warming starting in a cold climate state. Unfortunately, we lack insights in the mechanisms and environmental thresholds that forced the transition towards such a hothouse climate (Huber and Caballero, 2011). One of the most important reasons for this is that sedimentary archives that capture this time interval are scarce, also due to the low sea level.

From the above, questions were raised regarding the ice sheet presence, sea level change and relevant ecological response in not only the cool period and the following warming as well. In order to start providing more information on these questions, paleoclimate records were generated from Bass River and the North Sea basin in this study. A palynological study (notably dinoflagellates) were performed on both sites, thereby a sea level history and environmental changes around Atlantic margins were

reconstructed. Moreover, using organic geochemistry methods, SSTs were reconstructed from mid to late Paleocene on the sediments from a drill core from the New Jersey Shelf, USA (Bass River) which will be compared to existing SST records. The organic carbon isotopic results suggest a change in organic matter source. The negative excursions also reveal the latest Danian event and PETM. This study will shed a light on the paleoecological changes and a methane hydrates event coupling with temperature during the mid-Paleocene.
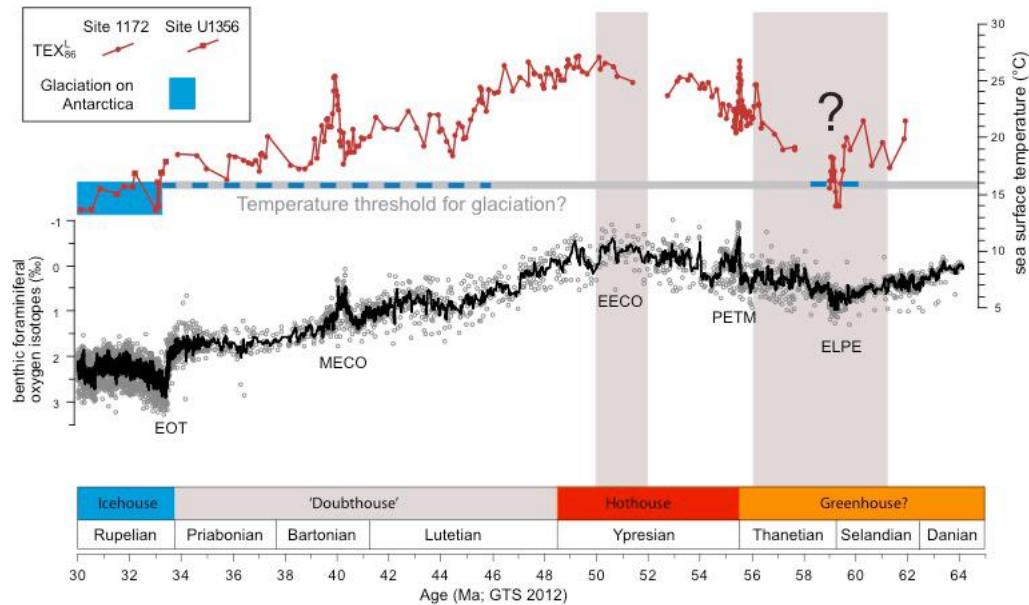


Figure 1 Adapted from Bijl, 2013 (personal communication) South Pacific (~65°S lat.) SSTs (calibrated by $TEX_{86}^{L}$; in red line with symbols, data dominantly from Bijl et al., 2009) and benthic foraminiferal stable oxygen isotopes stack

## 2. Background

### 2.1 Temperature evolution in the early Paleogene

The climate change during the Paleogene is a process from greenhouse to icehouse. The warm climate in late Cretaceous continued in the Paleocene. After the relative cold condition during the Maastrichtian, benthic oxygen isotopes excursed lighter indicating the warmest times of the Paleogene during the Paleocene and early Eocene. The temperature increased within tight range fluctuation and culminated at the boundary between the Paleocene and Eocene. On a shorter time scale, the Paleocene period contains a multi-million years reversal from cooling to warming (Cramwinckel, 2014). Benthic foraminifera shells were used to reconstruct deep ocean temperature. The $\delta^{18}O$ value of benthic foraminifera is mainly influenced by water temperature and sea water $\delta^{18}O$. These organisms produce $^{18}O$ depleted shells under warmer conditions. As sea water $\delta^{18}O$ is influenced by ice volume and salinity, foraminiferal oxygen isotopes are also depleted when the continental ice is little or absent (Emiliani, 1955). Sea surface temperatures (SSTs) are mainly reconstructed by the GDGTs derived from Archaea because the amount of pentacyclic carbons is influenced by the temperature (Schouten et al., 2002). Deep ocean temperature reconstructions based on benthic foraminiferal $\delta^{18}O$ from the central Pacific (Westerhold et al., 2011) show a clear cooling trend from the beginning of the Paleocene (~66 Ma) to the mid-Paleocene (~59 Ma). Temperature minimums were also discovered in South Atlantic deep water (Littler et al., 2014) and southwest Pacific SSTs (Bijl et al., 2009) around ~59-60 Ma.

The cooling trend did not continue after the mid-Paleocene climate minimum, on the contrary, it was followed by a warming trend towards the hot PETM and Early Eocene Climate Optimum (EECO) (Zachos et al. 2008). Many studies have focused on reconstructing the late Paleocene and early Eocene climate warming. The long-term negative excursion in benthic $\delta^{18}O$ indicates an approximate 7°C warming in both deep ocean (e.g. Zachos et al. 2001; Zachos et al. 2010; Cramer et al. 2009; Shackleton et al. 1986) and north Atlantic sea surface temperature (Sluijs et al., 2007). The warming was also exaggerated in high latitude sea surface water (Bijl et al., 2009, 2013; Frieling et al., 2014; Cramwinckel et al., 2018).

### 2.2 Carbon cycle in the Paleocene

Biogenetic organic carbon is usually $^{13}C$-depleted relative to atmospheric and oceanic inorganic carbon, because of a preferential fractionation for $^{12}C$ in bio-processes such as the photosynthesis. Variations in the carbon isotope ($\delta^{13}C$) of benthic foraminifera

is associated with the $\delta^{13}C$ of the surrounding sea water. As the ocean is a huge carbon pool, changes in oceanic $\delta^{13}C$ are influenced by OC burial, methanogenesis or oxidation, air-sea interaction etc. The fall in benthic foraminiferal $\delta^{13}C$ until 62Ma is concomitant with a relative warm deep ocean temperature in the early Paleocene (Zachos et al. 2008; Westerhold et al., 2011; Hollis et al., 2014). However, benthic foraminiferal $\delta^{13}C$ culminates at 57Ma and named as Paleocene carbon isotope maximum (PCIM). This event is characterized as the summit of $\delta^{13}C$ in the entire Cenozoic. From the PCIM onwards, $\delta^{13}C$ decreases gradually, concomitant with late Paleocene early Eocene warming. However, it should be noted that, unlike in the PETM or Eocene thermal maximum, the PCIM does not correspond to the $\delta^{18}O$ maximum and lags about 1.5 myr.

The PCIM is regarded as the consequence of a long-term elevated organic carbon burial rate (e.g. Shackleton, 1986; Thompson and Schmitz, 1997; Kurtz et al., 2003). The elevated burial of carbon in the ocean could cause a decrease in atmospheric $CO_2$ and a consequent global temperature decrease. There are organic rich sediments found in the South Pacific Ocean associated with PCIM (Hollis et al., 2014). These sediments are characterized by high TOC (0.5-10% wt.%) and high $\delta^{13}C_{org}$ (>−24‰). The mass erosion and organic sediments record an increase in terrigenous input, eutrophication and marine productivity. A short-lived Antarctic ice sheet was inferred based on the regression and low SSTs at ~59Ma.

After the PCIM, the warming couples a $\delta^{13}C$ decrease and carbonate compensation depth deepening. Carbon cycle modeling suggests that the depletion of $\delta^{13}C$ was mainly driven by the decrease in net organic carbon burial, however, it was also contributed by the elevated volcanic activity secondarily (Komar et al., 2013). The net organic burial decrease is predominantly caused by terrestrial organic matter oxidation (Kurtz et al., 2003) and marine $CH_4$ release (Dickens, 2003). As the continental shelf is the region with highest sedimentation rate (Duarte and Cebrian, 1996), it is the dominant burial environment for marine organic carbon (Hedges and Keil, 1995; Berner, 2006). Moreover, marine methane hydrates are predominantly stored on the slopes, the continental shelf is a significant $^{13}C$-depleted (-70‰) carbon (Komar et al., 2013) reservoir.

2.3 Paleocene climate events

Superimposed on the general climatic trends are several rapid hyperthermal events. The Dan-C2 event is characterized by a double negative excursion in both $\delta^{13}C$ and $\delta^{18}O$ at about 65.2Ma (Quillévéré et al., 2008). Latest Danian event (LDE) is recognized as a global transient warming episode at about 62.1 Ma (Bornemann et al., 2009; Westhold et al., 2011; Sprong et al., 2012). Early Latest Paleocene Event (ELPE) has been reported by Bernaola et al (2007) and Westerhold et al (2011). However, the evidences

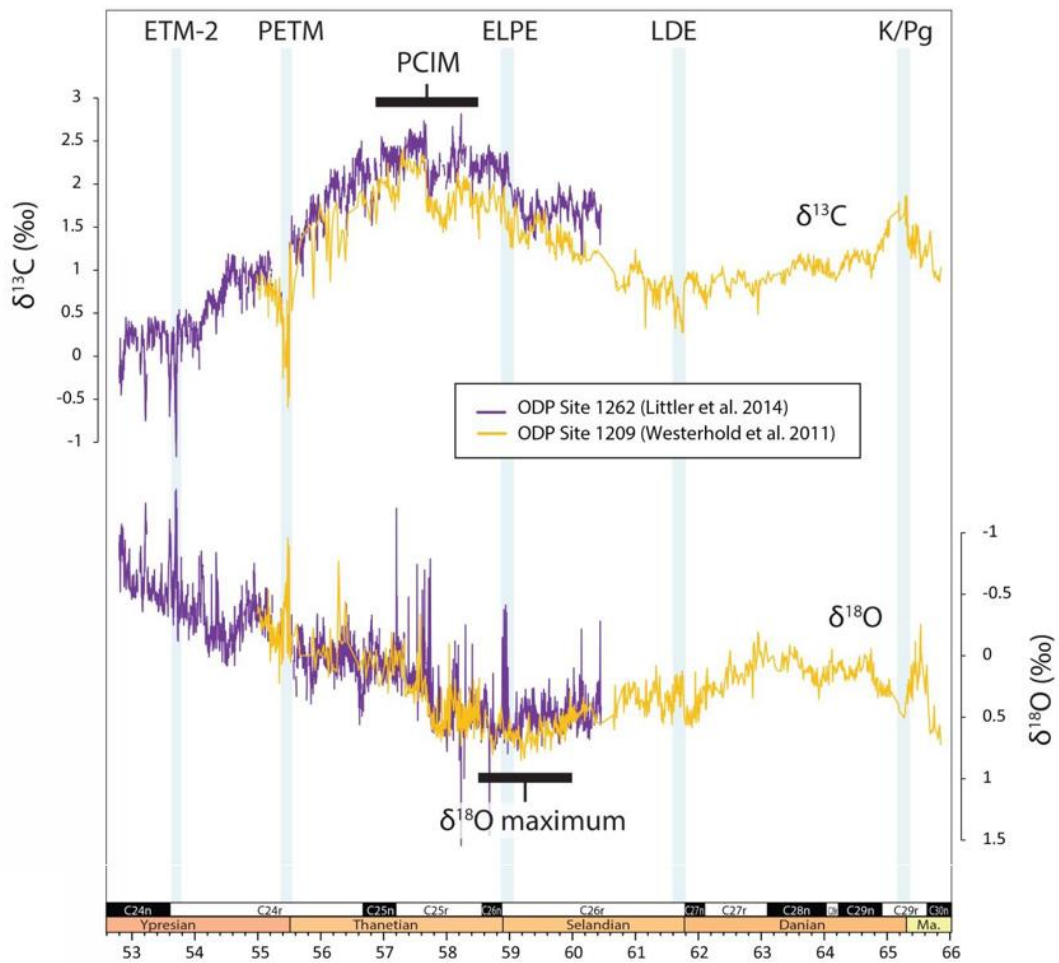are not sufficient enough to prove that it's a global hyperthermal event (Westerhold et al., 2011).



Figure 2   Paleocene-Early Eocene climate history. Benthic foraminiferal isotope records of 13C and 18O, climatic events are shadowed in light blue bars. Modified from Cramwinckel, 2014)

# 3. Materials and methods

## 3.1 Sampling

This study uses two successions of sediment records: Paleocene sections from North Sea basin drilled by Shell and lower Paleocene sections from ODP Leg 174AX Bass River core. 131 samples and 30 samples have been processed for $\delta^{13}C_{org}$ and palynology respectively from the North Sea basin. 28 samples and 40 samples have been processed for $TEX_{86}$ and palynology respectively from the Bass River.

The North Sea samples have been collected by P K. Bijl and J. Frieling in 2017. During the late Paleocene–early Eocene the North Sea was a restricted marine basin, characterized by high terrigenous input (Eldrett et al., 2014), principally from the Scotland– Faeroe–Shetland landmass (Knox 1998). Core 22/10a-5 is located in the central part of the basin (Figure. 3) close to core 22/10a-4 (Kender et al., 2012; Eldrett et al., 2014). The sediments depth is from 8502ft to 8883ft below sea floor including the Eocene-Paleocene boundary and late Cretaceous. There are approximately 60ft of shale that is laminated, organic rich and with greenish color which indicates the presence of glauconite in late Paleocene Lista formation. From 8560-8770ft, dark color and organic rich limestone dominates the content of the sediments, however, the continuity of limestone is sometimes interrupted by sandstone, shale and chalk. This limestione unit is recognized as Maureen formation. The section from 8770ft to 8845ft consists of sandstone with macroscopic quartz and feldspar, but there is an interval of limestone between 8812ft and 8828ft within. The underlying sediment which was considered as chalks in Ekofisk formation becomes light color, carbonate rich and there are black thin films inside (Figure 5).
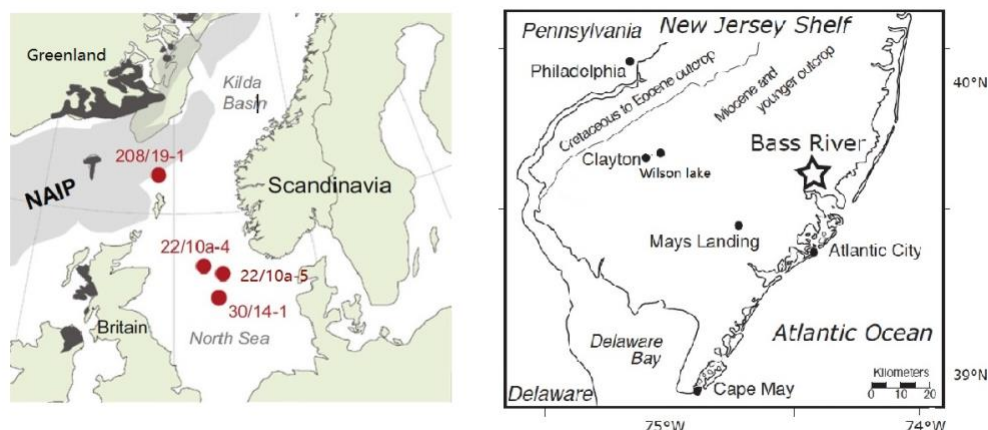


Figure 3 Localities of North Sea core 22/10a-5 and ODP 174AX bass River. Adapted from Kender et al., 2012; Sluijs et al., 2009

The Bass River core was drilled in Bass River State Forest, New Jersey, by ODP Leg174AX in 1996. This study used the samples from 1230ft to 1260ft from the lowest part of Vincetown Formation and Hornerstown Formation and 8 extra samples for paleotemperature reconstruction throughout the uppermost Vincetown Formation. At 1230-1231ft, macrofossils were found just below a peak in foraminiferal abundances. The underlying sediments became laminated and glauconite increasing until 1240.8ft. There is a subtle lithological change at this depth, which is from darker, more glauconite silt above to lighter, less glauconite clay below (Miller et al., 1998). This indicates an inconformity and hiatus and proved by foraminiferal biozones and calcareous nannofossil biozones (Liu et al., 1997). The section from 1240.8 to 1248.9 (378.20-380.66 m) consists of glauconitic quartzose silts. The section becomes increasingly glauconitic downsection, becoming glauconite sand from 1248.9 to 1258.7 ft, with fine quartz sand present below 1255 ft (Figure 5). Uppermost Paleocene sediments of the Vincetown Formation is relatively condensed (average sedimentation rates of 1 cm $kyr^{-1}$) and consist of glauconite-bearing siltstones, interpreted as a transgressive systems tract (Liu et al., 1997; Cramer et al., 1999)

## 3.3 Palynological preparation

All the samples were processed at Laboratory of Paleobotany and Palynology at Utrecht University. About 10g of the samples were crushed into 3-5mm size fragments and placed into centrifuge pots. 10% hydrochloric acid (HCl) was added until no more effervescent was observed after shaking, ensuring the complete dissolution of calcium carbonate, preventing the formation of calcium fluoride in following steps which can hinder the dissolution of silica. The liquid was decanted after still standing over night then centrifuged and washed with water to remove $Ca^{2+}$ ions. To remove siliceous matter 40% hydrofluoric acid (HF) was added to the samples and the pots were kept shaking for 2 hours, then they were filled up with water and stood still overnight. After centrifuging, the liquid was decanted. To remove gel-like fluoro-compounds, 30% HCl was added and decanted after mixing and centrifuging. In order to remove the siliceous matter completely, the HF and 30% HCl step was repeated for one more time. All samples were filtered on nylon sieves with a mesh size of 10μm. The residues were finally transferred into glycerine water. Slides for optical microscope were prepared with glycerine gel and sealed with cover varnish.

A tablet which contains a known number of *Lycopodium* spores ($\bar{X}$=9666) was added into each pot to quantify the number of dinoflagellates per gram sediment. Through counting both the *Lycopodium* and dinoflagellates, the absolute dinoflagellates amount can be retrieved.

## 3.4 Microscopy and Microphotography

An Olympus model CX21FS1optical microscope was used for counting. The slides were scanned at magnifications of ×100, ×200 and ×400. For each sample about 200-500 dinoflagellates were examined. Microphotography was performed on a Leica DM2500 microscope, photos were taken at magnifications of ×400 and ×700.

## 3.5 Dinoflagellate cysts grouping and ecology reconstruction
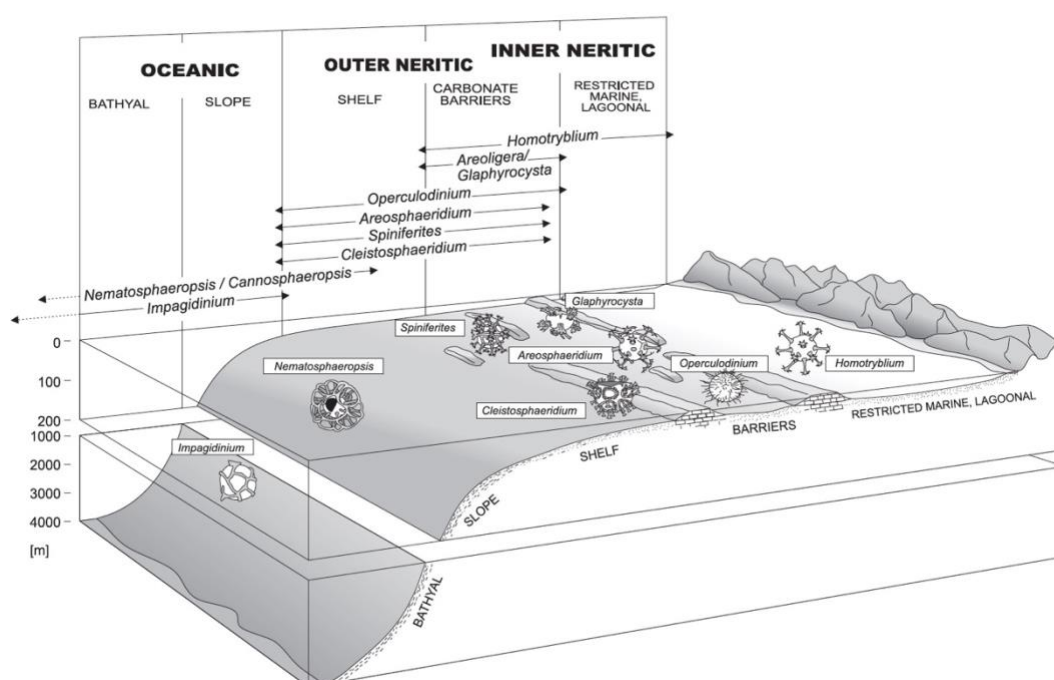


Figure 4 Schematic illustrations of dinoflagellates distribution along a proximal-coastal line Adapted from Sluijs et al., 2005

Dinoflagellates are a diverse group of unicellular eukaryotic phytoplankton with 2 flagella and a characteristic nucleus in marine settings (Fensome et al., 1993). There are both autotrophic and heterotrophic members. Although only 15-20% of living dinoflagellate species produce organic cellulose cyst (Fensome et al., 1996), the production of organic cysts can be tracked back to the motile stage of dinoflagellates. It is generally thought that the fossilized cysts are mainly produced during the sexual life cycle of dinoflagellates (Fensome et al., 1996) and various morphotypes can be related to certain physical, chemical, and ecological parameters of the water mass (Ellegaard, 2000). Therefore, fossilized dinocysts and its assemblage has been developed as an indicator of paleoecology such as sea level, salinity and productivity (e.g. Brinkhuis, 1994; Pröss and Brinkhuis, 2005; Sluijs et al., 2005). Ecological

interpretation of dinocyst assemblage data is often carried out by grouping cyst taxa that are considered to have similar ecological affinities and defining as a complex. Hereby, the complexes in this study follow Sluijs et al. (2005) and Sluijs & Brinkhuis (2009) for paleoecological interpretations and dinocyst grouping while species taxanomy follows Fensome and Williams (2004) and Evitt (1985).

Apart from the ecological complexes grouping, two other dinocyst-based ratios were also assessed. Heterotrophic organisms are often found in higher relative abundances in eutrophic areas, leading to the suggestion that these are indicative of eutrophication. The ratio of heterotrophic Peridinioid to autotrophic Gonyaulacoid cysts (P/G ratio) has been used to derive paleo-productivity patterns (Sluijs et al., 2005). But protoperidinoid dinoflagellates are a symbol of high productivity coastal and upwelling region (Firth and Clark, 1998; Prauss, 2001; Reichart and Brinkhuis, 2003), thus both Peridinioid and Protoperidinioid dinocysts were considered as heterotrophic P-cyst in this study. The ratio of neritic *Spiniferites* complex to inner neritic *Areoligera* complex has been developed as coastal proximity indicator by Sluijs et al (2008). The S/A index (*Spiniferites*/(*Spiniferites* + *Areoligera* )) can quantify the abundances of the two complexes, with the assumption that low S/A represents an inner neritic setting, while high S/A indicates an outer neritic setting.

3.6 Statistical analyses

To gain better insights in the paleo-ecological preferences of the dinoflagellates, statistical analyses were performed. In terms of statistical analyses, both principal component analysis (PCA) and canonical correspondence analysis (CCA) were performed using the paleontological statistics program C2 (Juggins, 2003) and PAST (Hammer et al., 2001) respectively. In the CCA, several organic geochemistry indexes were used as environmental parameters.

**Table1** Dinocysts complexes as environmental indicators found in this study

| Dinoflagellates cpx | Ecological settings |
| --- | --- |
| **Areoligera/Glaphrocysta cpx** *Areoligera, Glaphyrocysta, Adnatosphaeridinium* genera | Inner neritic (Powell et al., 1996) High energy marginal marine environments (Stover et al., 1996) |
| **Cordosphaeridinium cpx** *Cordosphaeridinium, Thalassiphora, Fibrocysta* genera | Open marine, neritic (Powell et al., 1996) |
| **Hystrichoshaeridinium cpx** *Hystrichosphaeridium ,* | Inner neritic (Powell et al. 1996) Possibly tolerant to swings in |

| | |
|---|---|
| *Oligosphaeridium* genera | salinity (Schiøler et al., 1997) |
| ***Spiniferites* cpx**<br>*Achomosphaera,*<br>*Spiniferites,*<br>*Spiniferella,*<br>*Hystrochostogylon,*<br>*Hafniasphaera* genera | Neritic to oceanic (Brinkhuis, 1994) |
| ***Apectodinium* cpx** | High temperature (Frieling et al., 2014), potential fresh water forcing (Kender et al., 2012) |
| ***Senegalinium* cpx**<br>*Senegalinium,*<br>*Phtanoperidinium.,*<br>*Deflandre,*<br>*Cerodinium.,*<br>*Spinidinium,*<br>*Palaeoperdinium* genera | Low salinity, eutrophication (Sluijs et al., 2005, 2009)<br>Remark: Palaeoperidinium is not included in the references above. However, it's a taxa related to fresh water pulse (Willumsen and Vajda 2010). |
| **Others**<br>The rest of species listed in Appendix 1 but not above | Uncertain |

## 3.7 Stable carbon isotope measurements

δ13Corg were measured on 131 samples from the North Sea basin. 0.2-0.3 g of the sediment powder of each sample was decalcified as follows: Samples were transferred to Greiner centrifuge tubes and decalcified by adding 7.5 ml 1M HCl. After shaking the tubes (110 times per minute) for 4 hours, the tubes were centrifuged and decanted. Another 7.5ml HCl was added and the tubes were kept shaking on a shaking machine overnight. After washed by 10ml deionized water twice, the samples were dried in a 60 °C oven for 3 days.

Subsequently, samples were measured for carbon isotopes on a ThermoScientific DeltaV Advantage coupled to a ThermoScientific Flash 2000 elemental analyzer at the Royal Netherlands Institute for Sea Research (NIOZ).

## 3.8 Organic geochemistry analysis

28 sediment samples were prepared at the Organic Geochemistry lab at Utrecht University. The total lipids of 10 grams of powdered sediments were extracted by an Accelerated Solvent Extraction machine by dichloromethane (DCM): methanol (9: 1/v:

v). An empirical amount of diatom earth was added to sediment powder to increase the permeability in order to maximize extraction efficiency. The total lipid extracts were concentrated and transferred to weighed 5ml glass vials and dried under $N_2$ flow.

In order to isolate the polar compounds GDGTs, apolar, ketone and polar fractions were separated through a chromatography column filled with activated aluminiumoxide by hexane: DCM (9:1/v: v), hexane: DCM (1:1/v: v) and DCM: methanol (1:1/v: v), respectively. A 9.9ng of $C_{46}$-GDGT as internal standard was added to every polar fraction for quantifications of GDGTs. Before testing, the GDGTs were filtered through 0.45μm PTFE filters with a hexane: isopropanol (99:1/ v: v) solvent.

GDGTs measurements were performed using High Performance-Liquid Chromatography-Mass Spectrometry (HP-LC-MS) with an Agilent 1260 UHPLC coupled to a 6130 quadrupole MSD as described by Hopmans *et al.* (2016) at NIOZ (8 samples) and Utrecht University (20 samples) respectively. Comparability between the output of the machines was tested and was good. Two Ultra High Performance-Liquid Chromatography (UHPLC) silica columns combined with a 2.1 x 5 mm silica pre-column were applied to separate fractions in approximately 5 μl of sample, at a constant 30 °C. Elution of GDGTs was performed with a mobile phase composition of 18% hexane: isopropanol (9:1/ v: v) relative to hexane for 25 minutes, linearly increasing to 35% in the following 25 minutes, finally linearly increasing to 100% in 30 minutes with a flow rate of 0.2 ml/min and a maximum back pressure of 230 bar. Run time was 90 minutes, re-equilibration time 20 minutes.

TEX$_{86}$

Sea surface temperatures (SSTs) were calculated from a GDGTs proxy TEX$_{86}$ using the calibrations of Kim et al (2010). The TEX$_{86}$ index is calculated by the relative abundance of isoprenoid GDGTs (Schouten et al., 2002):

$$\text{TEX}_{86} = \frac{\text{GDGT} - 2 + \text{GDGT} - 3 + \text{Cren}'}{\text{GDGT} - 1 + \text{GDGT} - 2 + \text{GDGT} - 3 + \text{Cren}'}$$

And the calibrations correlate with SST used in this study are (Kim et al., 2010):

$$TEX_{86}^{L} = \log(\frac{\text{GDGT} - 2}{\text{GDGT} - 1 + \text{GDGT} - 2 + \text{GDGT} - 3})$$

$$\text{SST} = 67.5 \times \text{TEX}_{86}^{\text{L}} + 46.9$$

$$TEX_{86}^{H} = \log(\frac{\text{GDGT} - 2 + \text{GDGT} - 3 + \text{Cren}'}{\text{GDGT} - 1 + \text{GDGT} - 2 + \text{GDGT} - 3 + \text{Cren}'})$$

$$\text{SST} = 68.4 \times \text{TEX}_{86}^{\text{H}} + 38.6$$

The calibration accomplished by Kim et al (2010) offered the optimal solutions in different temperature range: TEX$_{86}^{\text{H}}$ is a logarithmic function of TEX$_{86}$, which excludes the (sub)polar conditions and is more suitable for reconstructing SST in

tropical oceans in the range of over 15°C. However, $TEX_{86}^{L}$ removed the regio-isomer crenarcheaol from the initial $TEX_{86}$ GDGTs assemblage and its calibration to SST is based on a global core-top sediment dataset that includes high-latitude locations (Kim et al., 2010). For biophysical and analytical reasons, logarithmic $TEX_{86}^{H}$ is used to estimate the green house temperature at Bass River (Cramwinckle et al., 2018).

BIT

The branched and isoprenoid tetraether (BIT) index indicates to what extent the sample has been contributed by terrestrial input. It describes the relative contribution of marine and terrestrial types of membrane lipids known as glycerol dialkyl glycerol tetra-ethers (GDGTs). It is calculated based on the relative proportion of marine isoprenoid GDGTs and terrestrial branched GDGTs, according to the following equation:

$$BIT = \frac{I + II + III}{I + II + III + Cren}$$

A BIT index of 0 indicates no GDGTs of terrestrial origin, while a BIT index of 1 indicates all GDGTs are terrestrially derived. I, II and III are branched GDGTs (brGDGTs), primarily produced by terrestrial soil microbes, Cren is isoprenoid Crenarchaeol, >99% produced by marine crenarchaeota (Hopmans et al., 2004). However, there are recent studies indicating that in-situ production of brGDGTs in shelf sediments is a widespread phenomenon (Sinninge Damsté, 2016).

Methane index

Isoprenoid GDGTs produced by organisms other than Thaumarchaeota can cause a bias on $TEX_{86}$ SST reconstructions. For instance, $TEX_{86}$ is not applicable to high anaerobic methane oxidation rate sites (Schouten et al., 2002) which is dominated by Anaerobic Methanotrophic archaea (ANME) and sulfate reducing bacteria in Sulfate-Methane Transition Zones (SMTZ) (Hinrichs et al., 2009). In order to quantify the relative contribution of methanotrophic *Euryarchaeota* preferentially producing GDGT-1, -2 and -3 (Pancost et al., 2001) against planktonic and possibly benthic *Crenarchaeota* represented by crenarchaeol and its regioisomer (Sinnighe Damste et al., 2002) in the sediment GDGT pool, Methane Index (MI) was developed by Zhang et al. (2011):

$$MI = \frac{GDGT-1 + GDGT-2 + GDGT-3}{GDGT-1 + GDGT-2 + GDGT-3 + Cren + Cren'}$$

If the MI values are smaller 0.3, the samples can be regarded as normal marine sediments.

Ring index

The ring index (RI), representing the average ring number on the measured GDGTs, can determine if $TEX_{86}$ temperature estimates are influenced by non-thermal factors and/or deviate from modern analogues. RI is defined as follows (Zhang et al., 2016):

$$RI = 0 \times [GDGT - 0] + 1 \times [GDGT - 1] + 2 \times [GDGT - 2] + 3 \times [GDGT - 3]$$
$$+ 4 \times [Cren] + 4 \times [Cren']$$

# 4.Results

## 4.1 Biostratigraphy and age model calibration

There are 3 existing systematic biostratigraphy model Heilmann-Clausen (1985), Powell et al (1992) and Mudge et al (1996) used in this study, however, they are all based on an out of date time scale. This study on North Sea basin has recognized 12 key dinocyst events that can be used for the biostratigraphy calibration and age model establishment. The palynological events containin the first, last and abundant occurrence of certain dinocysts and they are correlated to the standard nannoplankton (NP) and planktonic foraminiferal (P) zone datums directly and calibrated to *Geological Time Scale 2012* (Gradstein et al., 2012), consequently, an age model was developed.
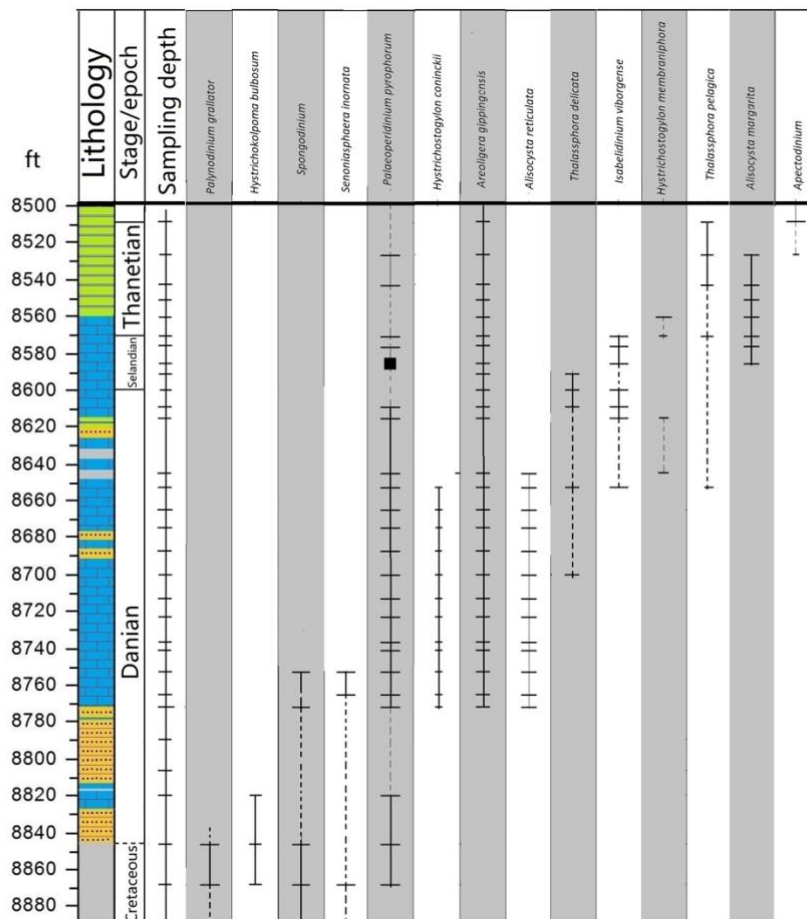


Figure 5 Paleocene dinocyst biostratigraphy markers, sampling depths, bio zonation, lithology plotted against time and core depth for Core 22/10a-5. Calibrated to GTS 2012 (Gradstein et al., 2012)

Table2 Dinoflagellates events and depth in Core 22/10a-5
7

| Dinoflagellates events | Depth |
|---|---|
| Last occurrence of *Palynodinium grallator* | 8847.05ft |
| First occurrence of *Alisocysta reticulata* | 8772ft |
| Last occurrence of *Senoniasphaera inornata* | 8752ft |
| Last occurrence of *Alisocysta reticulata* | 8643ft |
| Last occurrence of *Thalassphora* cf. *delicata* | 8601ft |
| First occurrence of *Alisocysta margarita* and abundant occurrence of *Paleoperidinium pyrophorum* | 8586ft |
| Last occurrence of *Isabelidinium*? *viborgense* | 8571ft |
| Consistent last occurrence of *P. pyrophorum* | 8569.5ft |
| First occurrence of *Apectodinium homomorphum* and last occurrence of *Alisocysta margarita* | 8527.5ft |
| First occurrence of *Apectodinium augustum* | 8508.8ft |

## 4.2 Stable carbon isotopes
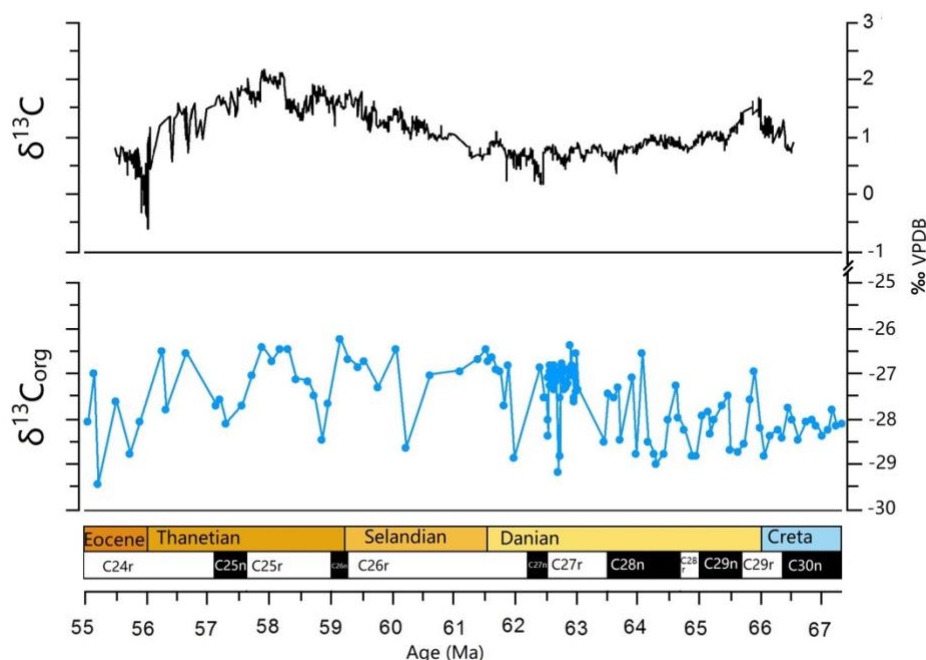


Figure 6 $\delta^{13}C_{org}$ results of Core 22/20a-5 against age (blue line with symbols), compare to benthic $\delta^{13}C$ (Westerhold et al., 2011) (black line).

Stable carbon isotope of organic matters from the Paleocene section of the North Sea site are presented versus age in Figure 6, versus depth together with dinocyst assemblage in Figure 8. Generally, the data of this site does resemble the long-term trend of benthic stable carbon results of Westerhold et al (2011) or Zachos et al (2008) but not there is high-amplitude scatter in the record which obscures clear visibility of these trends. In the late Maastrichtian chalk sediments, the $\delta^{13}C_{org}$ value is around -28‰. It shows a positive 2‰ shift as striding the K/T boundary. The positive CIE has been previously recognized at ODP Site 577 and Site 1209 (Zachos et al., 1989; Westerhold et al., 2011). Although the Cretaceous-Paleogene boundary is marked by a 2-3‰ negative carbon isotopic excursion in calcite and organic matters in the ejecta layer (Vellekoop et al., 2015, 2016), the negative CIE was not discovered due to sampling resolution.

In Danian stage, $\delta^{13}C_{org}$ maintained relatively negative values, varing from -27~-29‰. However, the slight decrease trend of $\delta^{13}C$ occurred in other sites was not recognized in this study. The relatively negative $\delta^{13}C_{org}$ culminated at 62.7 and 62 Ma with ~2‰ negative excursions. The time period about 62Ma is close to the correlative level of the base of C26r slightly preceding the Selandian (Bornemann *et al.,* 2009; Westerhold *et al.,* 2011).

In the Selandian and Thanetian epochs, $\delta^{13}C_{org}$ does not show any long-term rise or

decline, however, it becomes less depleted since 62Ma. After Danian the $\delta^{13}C_{org}$ oscillates between -26~-28‰, and forms four ~1.5Myr cycles until the boundary of Paleocene and Eocene. The $\delta^{13}C_{org}$ record of study ends up with the abrupt negative excursion (~3%)

4.3 Organic geochemistry

Organic geochemical processing was only carried out on the Bass River sediments. The sediments from the North Sea are too thermally matured to yield GDGTs data. Absolute amounts of GDGTs were not high, however, ranging between a total GDGTs weight of 50-170ng per gram dry sediment and dominated by iGDGTs.
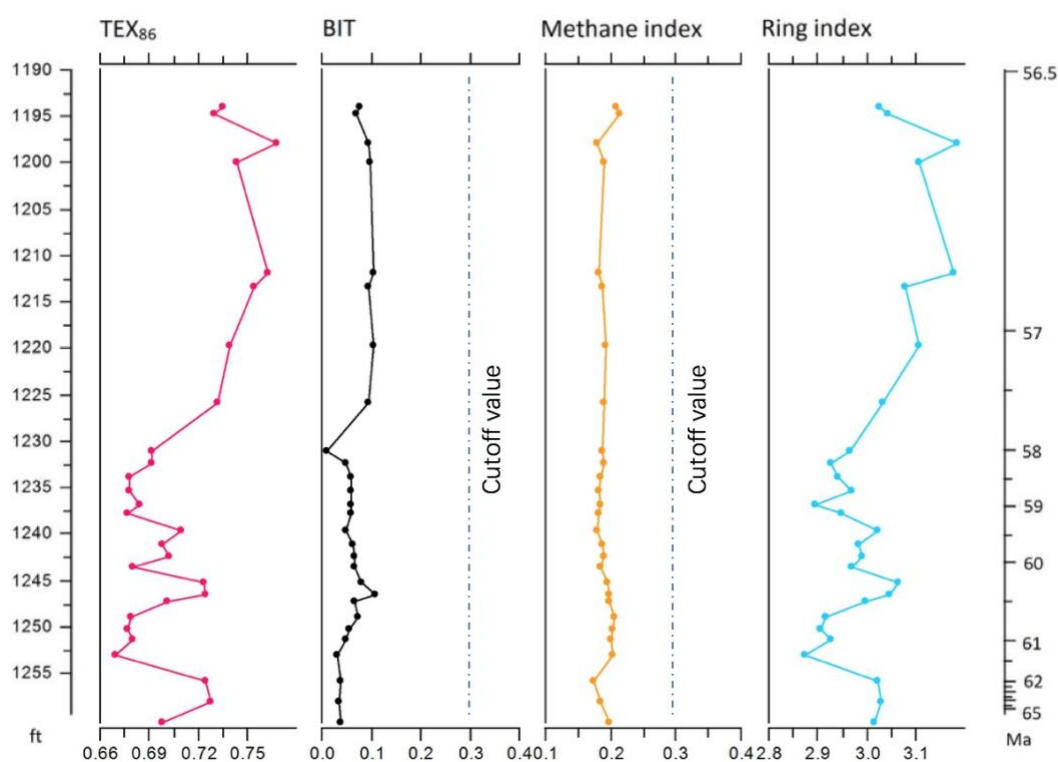


Figure 7 GDGTs proxies TEX86 (pink line), BIT (black line), MI (yellow line), RI (blue line) derived from ODP 174AX Bass River

BIT values vary from 0.03 to 0.11, which are low values indicating very limited terrestrial input. Methane index ranges within 0.17-0.21, not exceeding the normal marine environment threshold of 0.3. Hence, the temperature reconstruction based on $TEX_{86}$ is reliable on the Bass River site. $TEX_{86}^H$ and $TEX_{86}^L$ are correlated with BIT with $R^2 = 0.39$ and $R^2 = 0.29$ respectively (in supplementary files). $TEX_{86}^L$ reconstructed SSTs are around 7°C lower on average. High BIT values are associated with high $TEX_{86}$ and both calibrations in the Paleocene are applicable. For inter-site comparison, $TEX_{86}^H$ is used for temperature reconstruction.

TEX$_{86}$ proxy varies from 0.67 to 0.76, which corresponds to temperature range 26-31±4℃ by TEX$_{86}^{H}$ calibration. In the early Paleocene, the reconstructed SST was around 29℃. Due to 2 hiatuses in Danian stage, the record of early Paleocene is not complete, however, a significant 2℃ temperature drop occurred in mid Paleocene around 61.05 Ma. Although the temperature between 60.5Ma and 59.3Ma showed a fluctuation and recovered to 29℃ temporarily, it remained around 27℃ until 58.4Ma. Following the relatively cool time period, late Paleocene temperature increased steadily to 30℃ towards PETM. LDE cannot be recognized from the Bass River core. The time period about 62Ma close to the base of C26r (Bornemann *et al.,* 2009; Westerhold *et al.,* 2011) locates in a hiatus. While the event ELPE locates in the cool period (27℃) around 59Ma (Bernaola et al., 2007).

This study also provides a chance to connect the TEX$_{86}$ records around K/T boundary (Vellekoop et al., 2016) and PETM (Sluijs et al., 2007) together consequently retrieve a continuous paleotemperature record from late Cretaceous to early Eocene. The paleotemperature dropped from late Cretaceous (66.2Ma) 29℃ to early Paleocene 25℃, but also experienced an 22℃ impact-winter at 66.04Ma. The temperature early and mid-Paleocene fluctuated between 27~30℃ and increased to over 33℃ during PETM.

4.4 Palynology assemblages and statistical analyses

North Sea basin
Species were grouped as described in the methods section. Distribution of grouped dinocysts against time and depth is shown in Figure 9. At this site, the dinocyst assemblage consists of *Spiniferites* complex (cpx), *Areoligera* cpx, *Hystrichosphaeridinium* cpx, *Cordosphaeridium* cpx, *Senegalinium* cpx and *Operculodinium centrocapum. Apectodinium* cpx is only present in the early Eocene shales. The absolute quantity of total dinocyst is about 1000-5000 per gram sediment in limestones, 250-1000 in shales and chalks, however, falls into single digits in sandstones. The relative abundance changes of *Spiniferites* cpx (outer neritic), *Areoligera* cpx (inner neritic) can indicate the sea level change throughout Paleocene as well as other complexes such as *Hystrichosphaeridinium* and *Cordosphaeridium* which inhabited transitional sea level environments. The peridinioid/protopeidinoid cysts are dominated by *Senegalinium* complex in which the species *Paleoperidinium phyrophorum* contributes the most. An acme of *Paleoperidinium phyrophorum* (up to 80%) is also found at 8565ft depth (59.4Ma) together with a large amount of bisaccate *Pinus* pollen. Generally, at this site, the terrestrial palynomorph abundances are very low, this anomaly can reveal a low sea level and high freshwater input period.

Spiniferites complex (cpx) is the dominant contributor to the outer neritic group, thereby causing a dominant outer neritic signal throughout the record. In the intervals

8550-8586ft, 8653-8687ft and 8741-8752ft, there are peaks of *Spiniferites* cpx abundance. At the same time, *Areoligera* cpx decreases in abundance. This sea level change signal can be emphasized by S/(S+A) index (Figure 16). Together with the *Hystrichosphaeridinium* cpx abundance, the abundant presence of these three complexes occurs in order, which can reveal the 3 major sea level transgressive-regressive cycles.

The PCA analyses on relative abundance clearly separated *Spiniferites*, *Hystrichosphaeridinium*, *Cordosphaeridium*, *Areoligera* and *Senegalinium* along axis 2 (Figure 11). *Spiniferites*, *Senegalinium and Operculodinium* are mainly separated along axis 1. However, due to the short-term occurrence and limited abundance, *Apectodinium* species scores of both components are very close to zero. Hence, in this PCA analysis, component 1 indicates the sea level and component 2 indicates the salinity. CCA analysis is carried out when $\delta^{13}C$ and carbonate concentration are considered as environmental factors. *Areoligera* complex is plotted close to $\delta^{13}C_{org}$, thus $\delta^{13}C_{org}$ can be related with a lower sea level. *Operculodinium* and other taxa are plotted along the carbonate concentration, indicating that the other taxa are mainly correlated to an open ocean condition (Figure 12).

Bass River
The dinocyst assemblage recorded in Bass River is plotted against age and depth in Figure 9. The grey color shadowed data in late Paleocene was retrieved by Van De Wal (2011). There is less species diversity in the Bass River, the dinocysts are much better preserved than the North Sea material, probably because of the less-matured depositional history of the basin. Hence, some fragile and small size genera such as *Membranosphaeridinium* and *Eocladopyxis* are recognized. Early and mid-Paleocene assemblages are dominated by either typical open ocean *Spiniferites* or inner neritic *Areoligera*. The fluctuation pattern of both complexes is the same as in the North Sea. *Hystrichosphaeridinium* abundance is generally lower than 20%, but it increased to 40% between 1234.7ft and 1236.5ft which correlates a significant *Areoligera* decreasing and less *Spiniferites* period. The peak of *Operculodinium* occurs in the interval 1245.85-1254.95ft, correlating to a *Areoligera* decreasing and *Spiniferites* increasing period. *Senegalinium* and *Menbranosphaeridinium* are only abundant in the late Paleocene close to the PETM.

The PCA analyses of this site separated sea level indicators *Spiniferites* and *Areoligera* along axes 1 (Figure 11). Other common taxa mutually point to similar directions along component 2. In CCA analysis *Spiniferites* is plotted very close to TEX$_{86}$. However, other complexes did not show any significant correlation between the organic geochemistry indexes. However, in the CCA analysis performed by Sluijs and Brinkhuis (2009) on the PETM interval from the same core, *Spinifeites* was not correlated to any environmental parameters (Figure 12).
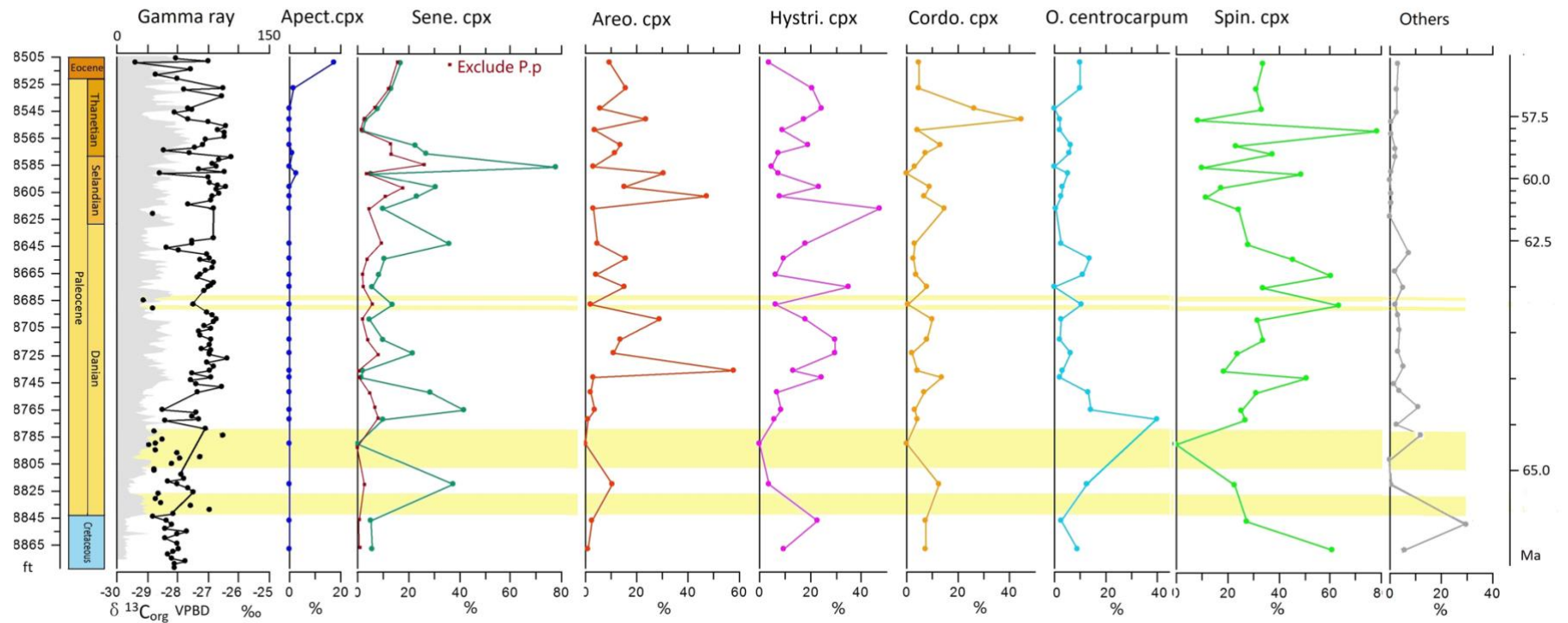
Figure 8 Paleocene dinocysts assemblage at North Sea Core 22/10a-5 against depth and age as secondary y-axis; together with gamma ray results (grey shadow), d13Corg (black line with symbols), yellow shadow represents sandy samples, dinocysts grouped in complexes according to Sluijs et al., (2009)
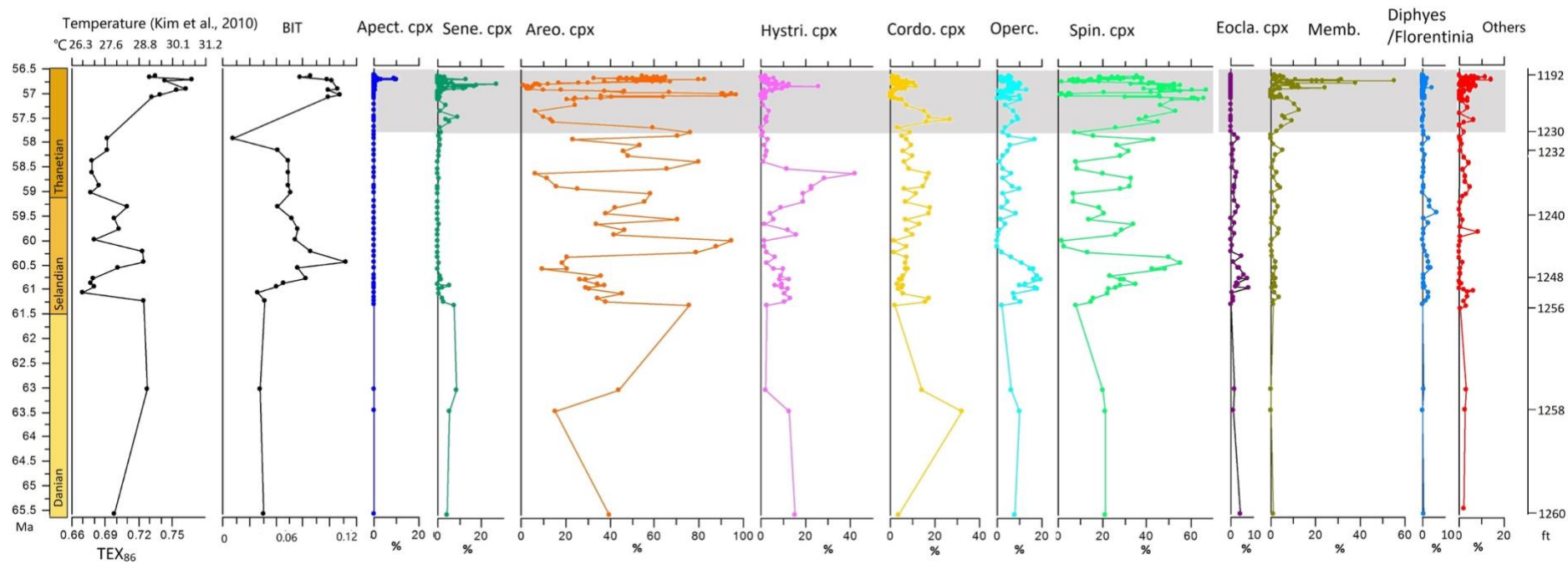
Figure 9 Paleocene dinocyst assemblage at ODP 174AX Bass River against age and depth as secondary y-axis, together with SST calibrated by TEX$_{86}$$^{H}$ and BIT, grey shadowed dataset was processed by Van Der Wal, 2011, Dinocysts grouped in complexes according to Sluijs et al., (2009)
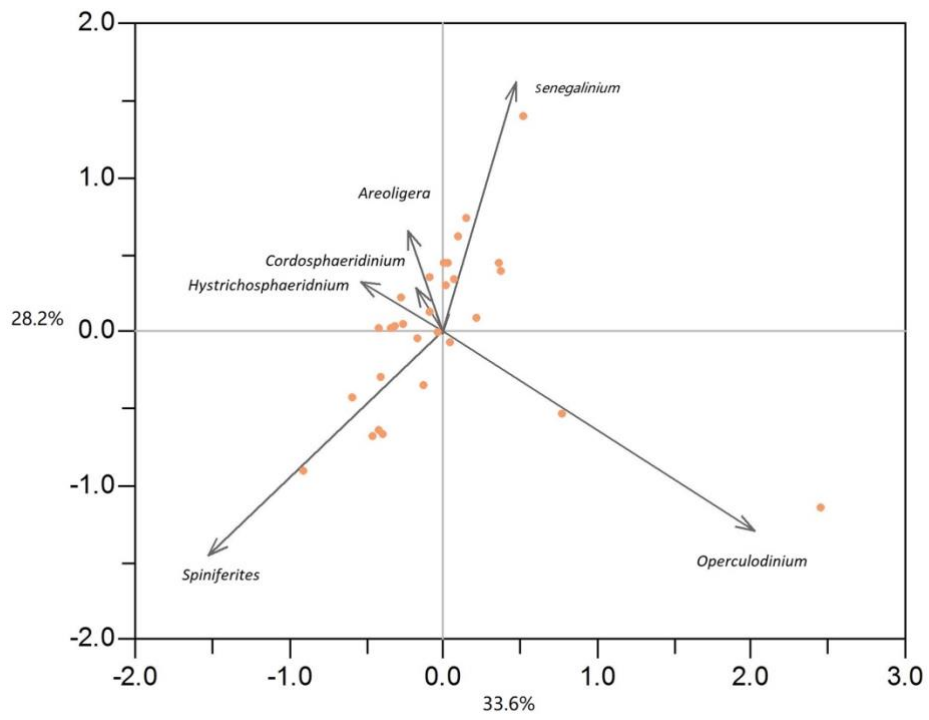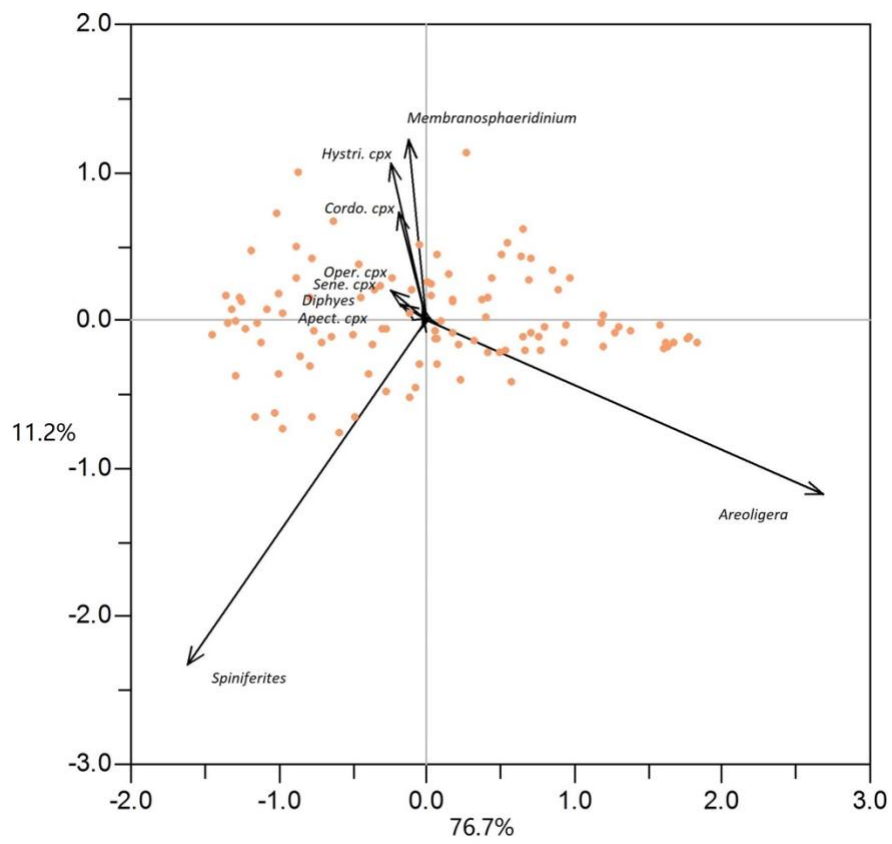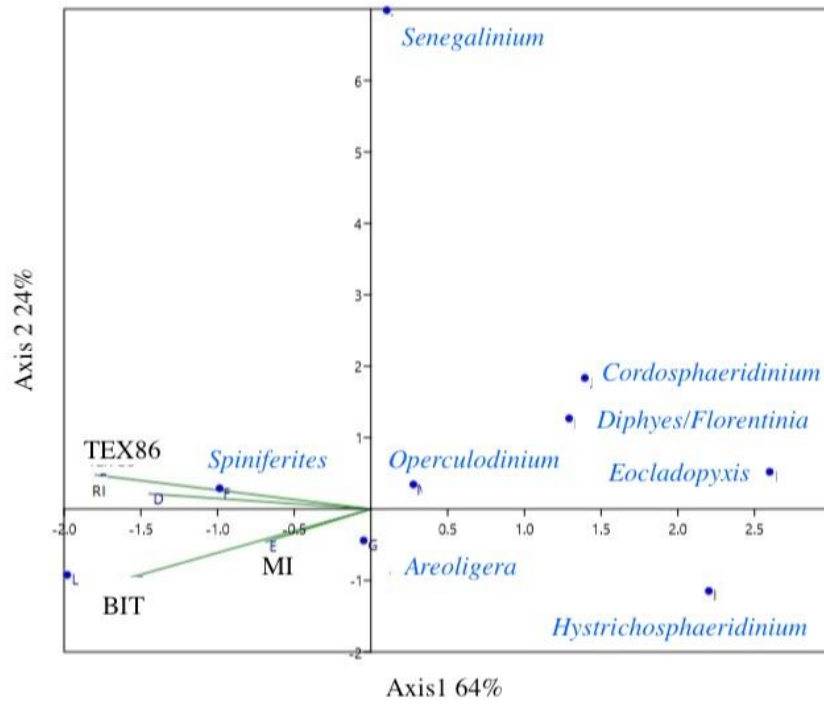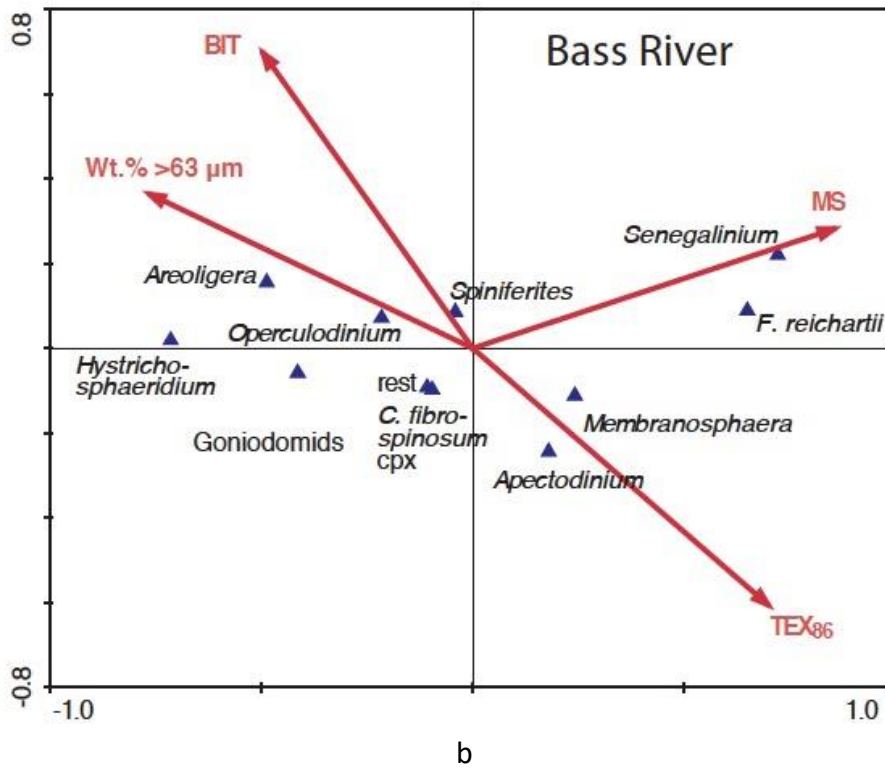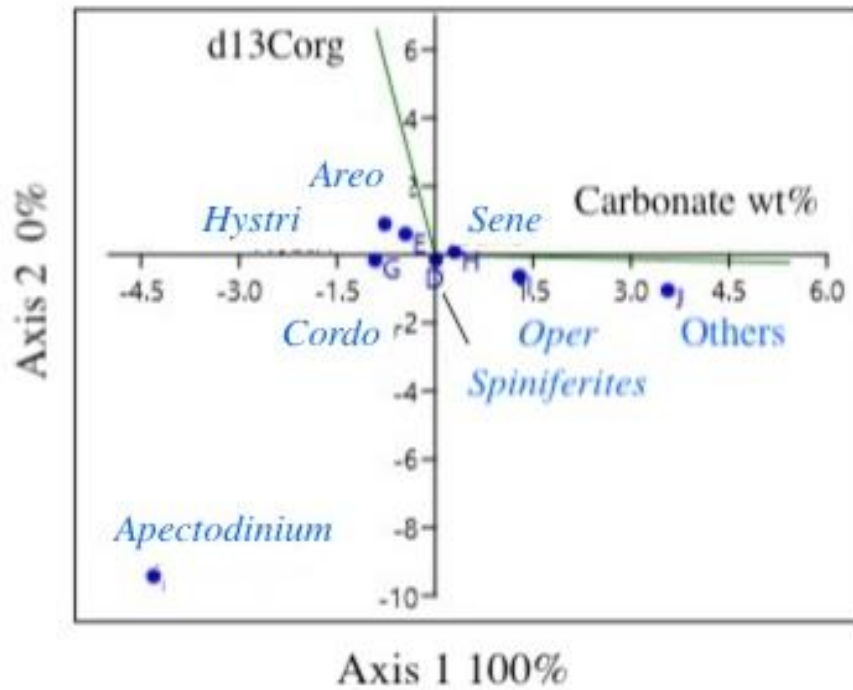
Figure 10 PCA analysis of Core 22/10a-5



Figure 11 PCA analysis of ODP 174AX

a



b

c

Figure 12 a: CCA analysis of ODP 174AX Paleocene section b: ODP 174AX PETM section (Adapted from Sluijs et al., 2009) c: CCA analysis of Core 22/10a-5

**5.Discussion:**

5.1 Age model

Last occurrence of *Palynodinium grallator*
Calibration: Late Cretaceous, equivalent to the base of NP1 and P0, 66.04Ma
Remarks: The last occurrence of *P. grallator* locates at 8847.05ft in the light color chalk. *P. grallator* is a typical Cretaceous Maastrichtian dinoflagellate cyst (Costa and Davey 1992). It first occurs consistently within the Maastrichtian, distribute in a large area on the European mainland and in the North Sea Basin (Powell et al., 1992 and refs therein). The extinction of *P. grallator* is considered to be the top of Maastrichtian and the end of Cretaceous (Powell et al., 1992). Another late Cretaceous dinoflagellate *Spongodinium delitiense* was also found in the chalk samples by this study but also seen together with *Senoniasphaera inornata*, a Paleocene dinocyst (Mudge et al., 1996). This is thought to be reworked. In this case, the last occurrence of *P. grallator* is regarded as the first bio-datum indicating the boundary of Cretaceous and Paleocene in this study.

First occurrence of *Alisocysta reticulata*
Calibration: Mid Danian, equivalent to the interface of P1b and P1c, 63.9Ma
Remarks: The first occurrence of *Alisocysta reticulata* locates at 8772ft. It is coincident with the dinoflagellate biozone definer *Hafniasphaera cryptovesiculatus* Williams 1998 (Powell et al., 1992 described as *Spiniferites cryptovesiculatus*) while Heilmann-Clausen (1985) and Mudge et al (1996) did not calibrated this event. The *Hafniasphaera* genus is widely but barrenly distributed throughout the Paleocene sediments, due to the reworked sediments and relatively dark morphology, the species of *H. cryptovesiculatus* and *H. septata* were not distinguished in this study. Therefore, the first occurrence of *A. reticulata* was calibrated to the boundary of P1b and P1c, 63.9Ma.

Last occurrence of *Senoniasphaera inornata*
Calibration: Mid Danian, equivalent to lowest NP4 and within P1c, 63Ma
Remarks: The last occurrence of *S. inornata* locates at 8752.5ft. The calibration of this event became complicated due to the different results in Mudge et al (1996) and Powell et al (1992) and the lack of record in Heilmann-Clausen (1985). Hereby, this study followed the biostratigraphy of Powell et al (1992) since this is an uncertainty indicated by Mudge et al (1996) and calibrated this event to lowest NP4 and within P1c.

Last occurrence of *Alisocysta reticulata*
Calibration: Upper Danian, mid NP4 and mid P2, 62.5Ma
Remarks: The last occurrence of *Alisocysta reticulata* locates at 8643ft. Since the calibrations of Powell et al (1992) and Mudge et al (1996) corelates to each other, this

study followed their result.

Last occurrence of *Thalassphora* cf. *delicata*
Calibration: Lowest Selandian, equivalent to the boundary of NP4-NP5 and around the boundary of P3a and P3b, 61.51Ma
Remarks: This study merged *Thalassphora* cf. *delicate* and *Thalassphora delicata* together. *Thalassphora* cf. *delicata* is distinguished from *Thalassphora delicata* by the presence of large regular openings in the periphram and typically occurs with *Paleoperidinium pyrophorum* dominating assemblages (Mudge et al., 1996). However, in these North Sea sediments, no *Thalassphora* cf. *delicata* or *Thalassphora delicata* were witnessed in *P. pyrophorum* abundant (over 20%) assemblages. Furthermore, the distribution of *Thalassphora delicata* is from Paleocene-Eocene boundary (Powell et al., 1992), which is not found in this study either. After integrating the present information and evidences, this event was calibrated to the boundary of NP4-NP5 at 8601ft but with lower priority.

First occurrence of *Alisocysta margarita* and abundant occurrence of *Paleoperidinium pyrophorum*
Calibration: Selandian, equivalent to the boundary of NP5-NP6, 59.54Ma
Remarks: The first occurrence of *Alisocysta margarita* is not marked by Mudge et al (1996), while Powell et al (1992) calibrated it to the boundary of NP5 and NP6. Heilmann-Clausen (1985) also reported some transitional specimens of genus *Alisocysta*, but they were not found by the palynological study on the North Sea samples. Hereby, the depth 8586ft is calibrated to 59.54Ma.

Last occurrence of *Isabelidinium*? *viborgense*
Calibration: early Thanetian, boundary between NP6 and NP7, 58.94Ma
Remarks: This event and the consistent last occurrence of *P. pyrophorum* were found in the same sample from the dept interval 8571-8568.7ft. According to the biostratigraphy by Heilmann-Clausen (1985), Powell et al (1992) and Mudge et al (1996), the last occurrence of *Isabelidinium*? *viborgense* was determined at the depth of 8571ft, calibrated to 58.94Ma.

Consistent last occurrence of *P. pyrophorum*
Calibration: early Thanetian, boundary between NP7 and NP8, 58.7Ma
Remarks: As described in last event, this event was assigned to the top of the sample interval which is 8568.7ft, calibrated to 58.7Ma. There are *P. pyrophorum* discovered in the shallower samples, but there is an absence in between. In this case only the end of consistency is defined as the last occurrence.

First occurrence of *Apectodinium homomorphum* and last occurrence of *Alisocysta margarita*.
Calibration: late Thanetian, boundary between NP8 and NP9, 57.21Ma
Remarks: These 2 events were found overlapped by Heilmann-Clausen (1985) while

Powell et al (1992) indicated a tiny lag of *A. homomorphum*'s first occurrence. This study defined the average depth 8527.5ft of this sample interval as the common datum of the 2 events, which can be calibrated to 57.21 Ma.

First occurrence of *Apectodinium augustum*
Calibration: Early Eocene, boundary of P5 and P6, 55.2Ma
Remarks: The first occurrence of *A. augustum* is calibrated to the onset of P6 by Heilmann-Clausen (1985) and Powell et al (1992). Sluijs et al (2007) suggested that the negative carbon isotope excursion (CIE) preceded the abundant occurrence of *Apectodinium* genus by ~5kyr. In this study the onset of abundant occurrence of *Apectodinium* was discovered together with the CIE in the sample interval of 8525.2-8528ft (core thickness is about 5cm) which results in a ~15kyr error. The order of CIE and *Apectodinium* occurrence can't be specified by this study due to the sampling resolution.
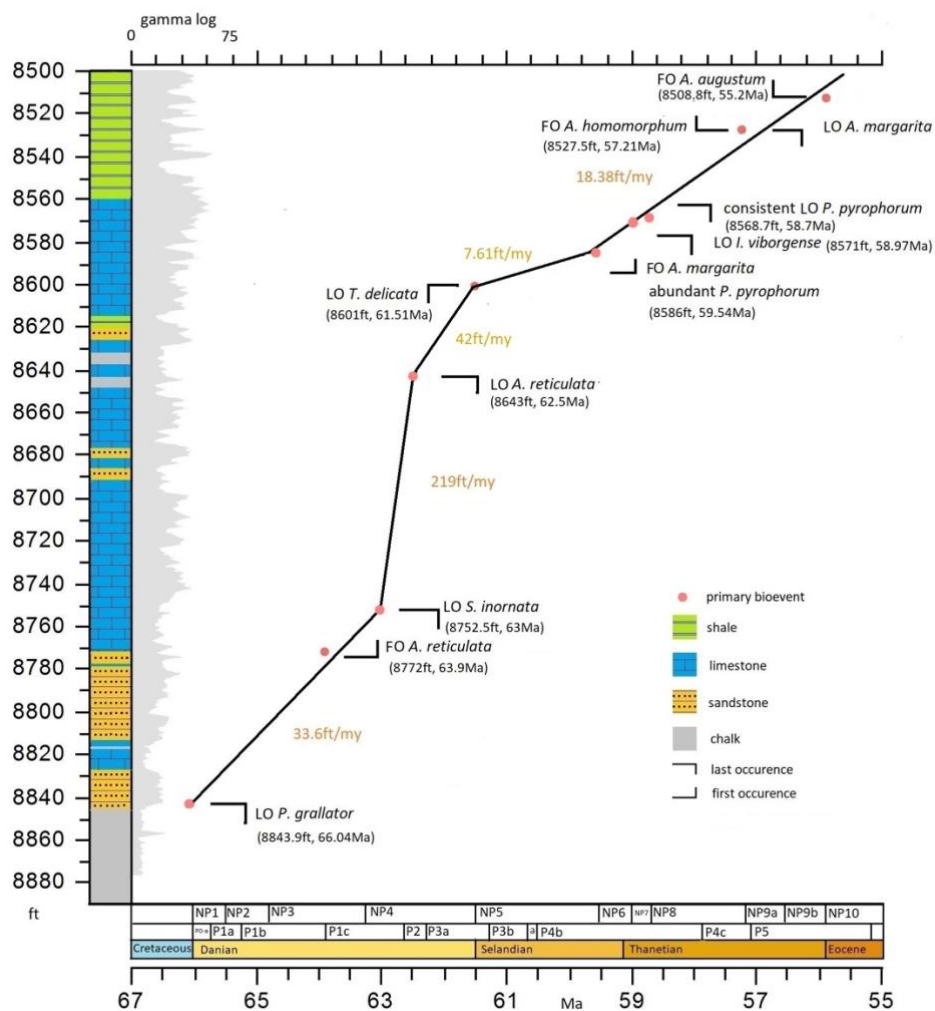


Figure 13 Age depth plots for Core 22/20a-5, grey shadow= gamma log, The line of correlation represents linear sediment accumulation rates, the sharp increase of sedimentation rate is due to unsampled sand. Calibrated to GTS 2012

Bass River

Only *Senoniasphaera inornata* was found in the Bass River core as a marker species due to the hiatus (Miller et al., 1998). Therefore, the age model of Bass River core is not based on the dinoflagellates biozones but on the standard nannoplankton and planktonic foraminiferal zone datums which were already determined by the Initial Reports 174AX (Miller et al., 1998). This study recalibrated these datums to GTS 2012 (Gradstein et al., 2012) and established a new age model for the lower section of the Paleocene sediments.
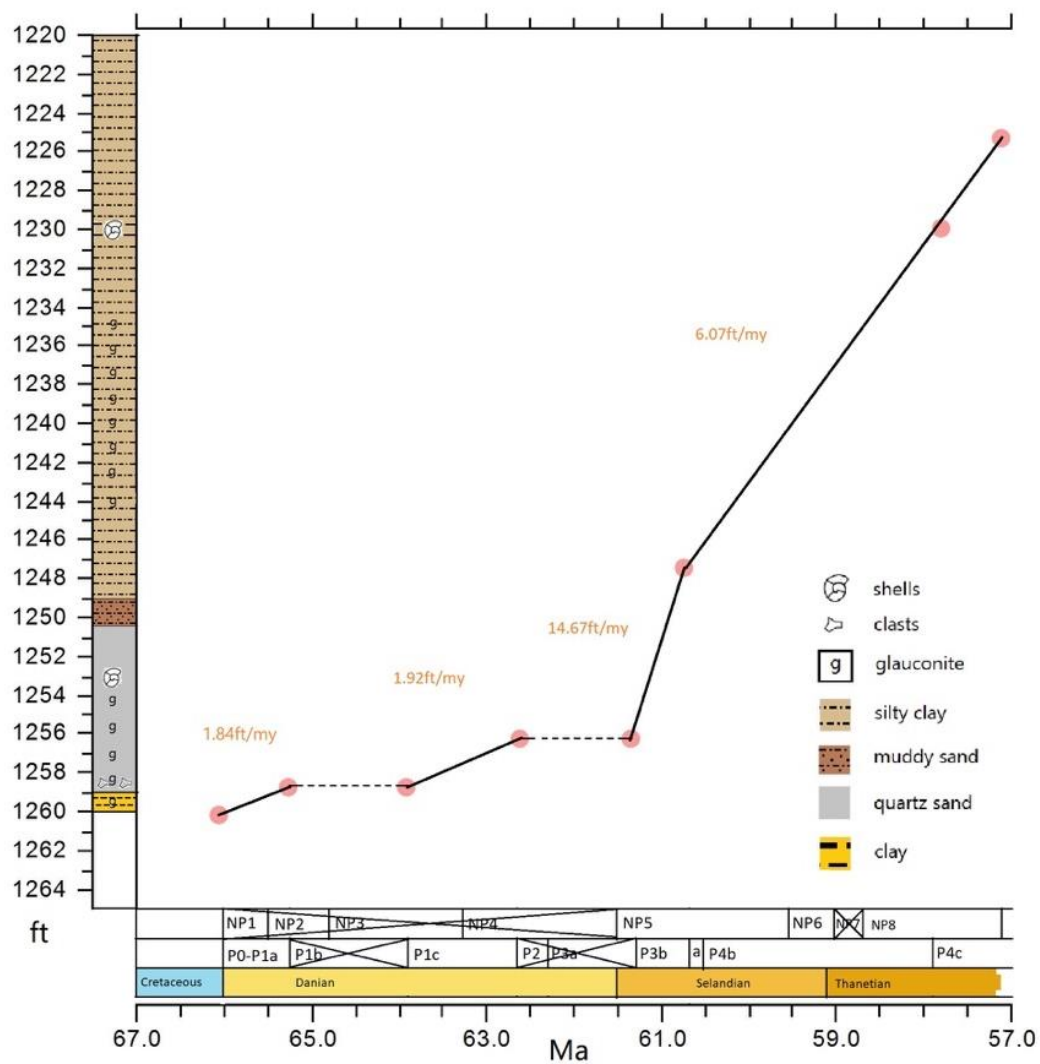


Figure 14 Age depth plots for ODP 174AX, The line of correlation represents linear sediment accumulation rates, crosses in biozonations represent they were not observed. Calibrated to GTS 2012

## 5.2 Key fluctuations in Paleocene $\delta^{13}C_{org}$ records

The change trend of the Paleocene $\delta^{13}C_{org}$ records discovered by this study at the North Sea basin core 22/10A-5 is ambiguous. Unlike the multi-million years $\delta^{13}C$ reversal found in benthic foraminifera (e.g., Zachos et al., 2001; Hollis et al., 2005; Westerhold et al., 2011; Hollis et al., 2014), there is high-amplitude scatter in the record which obscures clear visibility of these trends. However, the $\delta^{13}C_{org}$ values are lower in Danian, higher in Selandian and Thanetian, and highly depleted across the Paleocene-Eocene boundary.

Despite the vague changing trends, $\delta^{13}C_{org}$ values are also related to lithology. In the chalk and limestone sections, the $\delta^{13}C_{org}$ values are lower (-28‰), indicating that the organic matters are mainly contributed by marine biomass rather than terrestrial organic matter input (Dunkley et al., 2010). In the late Paleocene shales which contain more organic matter and plants fragments, $\delta^{13}C_{org}$ values are relatively higher (-27‰). This phenomenon is similar to the discovery in Kender et al (2012). But the shale sample with a significant negative excursion (-29.5‰) is more likely contributed by $^{13}C$-depleted carbon injection associated with PETM as *A. augustum* is recognized inside (Sluijs et al., 2007). Although coarse sand sediments were removed during sampling, there are still several Danian sandy clusters used for isotopical measurement and palynological study. $\delta^{13}C_{org}$ results in sandstones are particularly low, approaching -29‰. The only anomaly occurs in the sandy layer overlaying Cretaceous chalks. Within this cluster, $\delta^{13}C_{org}$ experiences an abrupt positive shift (-27‰) and drops to -29‰ immediately. Thus, these sandy sediments should not be regarded as low sea level high terrestrial input consequence, on the contrary, these are caused by turbidites (Kender et al., 2012; Jolly and Lonergan., 2002). Furthermore, neither marine dinoflagellates nor terrestrial pollens/spores were preserved in these samples. Thus the organic matter inside is dissolved organic matter which was produced after the rapid oxidation of methane. Turbidites also caused two negative carbon excursions in late Danian and the sedimentation rate in late Danian (64-61.5Ma) is very high due to rapid turbidites bias. A -2‰ excursion occurs at the boundary of C26r and C27n coincides the latest Danian event. The latest Danian event is a transient warming episode associated palaeoenvironmental changes that are similar to those for the PETM (Westerhold et al., 2008; Bornemann et al., 2009; Sprong et al., 2012). Huge amounts of isotopically light carbon may have been added to the ocean–atmosphere system, possibly as a result of the release and subsequent dissociation of methane, or alternatively through oxidation of terrestrial or marine organic carbon, or enhanced volcanic outgassing (e.g. Pagani et al., 2006; Sluijs et al., 2007). Hereby, the latest Danian event is supposed to be associated with the methane hydrates destabilization which can cause the turbidites as consequences (Kvenvolden., 1999).

In the Paleocene-Eocene junction samples, a 3‰ negative excursion occurred in the lithologically continuous samples. The global PETM CIE is determined by the negative excursion in both marine and terrestrial $\delta^{13}C$ between 2% and 7% (Schouten et al.,2007).

As the dinoyst *Apectodinium augustum* was also found sporadically in the most $^{13}$C-depleted sample (8508.8ft), the onset of the CIE is regarded as the Paleocene-Eocene boundary. However, through comparing the gamma ray results of this site and a parallel site 22/10a-4, the Paleocene-Eocene boundary should not be present in this depth theoretically. The gamma ray results of both cores indicated that the top sample of this study locates in the Lista formation while the PETM locates in the overlying Sele formation. Two plausible reasons can lead to this divergence. The first one is the error of gamma ray in a deep sediment depth, which implies that the age model in this study is reliable. The second possibility is that the *A. augustum* presence is false due to rework. In this way there is a significant pre-PETM CIE found at this site which is not recorded at the parallel site.

At site 22/10a-4, $\delta^{13}C_{org}$ results were also reported associated with palynological residues. More plant tissues can lead to consistently heavier $\delta^{13}C_{org}$ values (Jones et al., 2010; Kender et al., 2012). However, the isotopical result of the only terrestrial palynomorph rich sample (8586ft) does not show any positive shift standing out of the background.

Although the benthic carbon isotopes in late Paleocene early Eocene are related to both long and short eccentricity cycles (Lourens et al., 2005; Westerhold et al., 2008; Westerhold et al., 2011), due to sampling resolution this phenomenon could not be verified in this study. However, there is a 1.63 Myr cycle in $\delta^{13}C_{org}$ results, approximately 4 long eccentricity cycles, found after 62Ma. But the filtered $\delta^{13}C_{org}$ values did not reveal any maxima-minima corresponding relation which was found by Westerhold et al (2011).

5.3 Mid-Paleocene cooling and temporal spatial difference

Benthic foraminiferal $\delta^{18}O$ suggests that the cooling trend in Paleocene initiated at around 63 Ma and continued to the onset of ELPE event at around 58 Ma, therefore, implies a relative cool interval in the mid-Paleocene. The cool period is followed by the late Paleocene-early Eocene warming which was proved globally by both deep ocean temperature records derived from $\delta^{18}O$ (Zachos et al., 2008; Westerhold et al., 2011) and SST records derived from GDGTs (Bijl et al., 2013, 2009; Frieling et al., 2014; Hollis et al., 2014). The SST records derived from Bass River generally resemble the pattern above, however, display distinct change timing and amplitude.

There are two relatively cool periods found at Bass River. The SST decreased 2℃ since 61.05 Ma and maintained around 27℃ until 60.78 Ma. In the interval between 60.56 Ma and 59.31 Ma, the SST recovered to 28-29℃ as in the early Paleocene. From 59.03 Ma to 58.37 Ma is the second cool period locating in mid and earliest late Paleocene. Henceforth, SST rose by ~7℃ till PETM and reached 33℃ by TEX$_{86}$$^H$ calibration. The SST records at Bass River confirm the evidences of a cool mid-Paleocene. However, it also implies temporal and spatial differences comparing with other sites.

There are remarkable differences in the SST trends from the Northern Hemisphere. SSTs from the low latitude (20°N) North Atlantic region don't show obvious cooling trend in the Mid-Paleocene. On the contrary, SSTs were consistently high and similar to the SSTs in Eocene hyperthermal events (Cramwinckel, 2018; Pearson et al., 2007). TEX$_{86}$$^H$-derived SSTs at high latitude west Siberian section (60°N) decreased gradually since 60Ma to a minimum at 57.6Ma from 19℃ to 17℃ (Frieling et al., 2014). This cooling trend corresponds to what was found at Bass River in this study, however, there is a huge meridional gradient of 10℃ and a 0.8myr later of lowest temperature occurrence time. The situation in the southern hemisphere is different from that in the north. The SSTs in mid (Hollis et al., 2012, 2014) and high latitudes (Bijl et al., 2009, 2013) all entered a cool period between 58.9Ma and 58.4Ma. This concomitant cooling is also characterized by a highly reduced meridional gradient from 60°S to 50°S, thus implying an unbalanced thermal distribution in different hemispheres. A temporary presence of Antarctica ice sheet is indicated by Hollis et al (2014). Moreover, the temperature gradient will increase during warming due to polar amplitude (Cramwinckel et al., 2018). This reduced temperature gradient can be regarded a consequence of climate cooling. The cause of glaciation is still uncertain and enigmatic, some insights can be revealed by this phenomenon. Although very few $p$CO$_2$ records were reconstructed for the Paleocene and suffered from poor resolution and uncertainty (Zhang et al., 2013; Royer and Beerling, 2011; Pearson and Palmer, 2000), the potential glaciation lies in a low atmospheric CO$_2$ period. Meridional SST gradient can be reduced by the decline of $p$CO$_2$ and other mechanisms such as plate tectonics and cloud albedo (Fedorov et al., 2015, 2013). The glaciation thus can be a consequence of the synthesis of both $p$CO$_2$ decline and tectonic activity. Consequently, cold deep water formed from the high latitude Southern Ocean and proved by the identical trend of deep

ocean temperature (Westerhold et al., 2011). It is proven that there is a polar amplification during $p$CO$_2$ driven climate warming (Cramwinckel et al., 2018), however in the mid-Paleocene cooling event, high latitude behaved similar to mid-latitude in the northern hemisphere and in the southern hemisphere the meridional gradient reduced due to ice sheet formation.
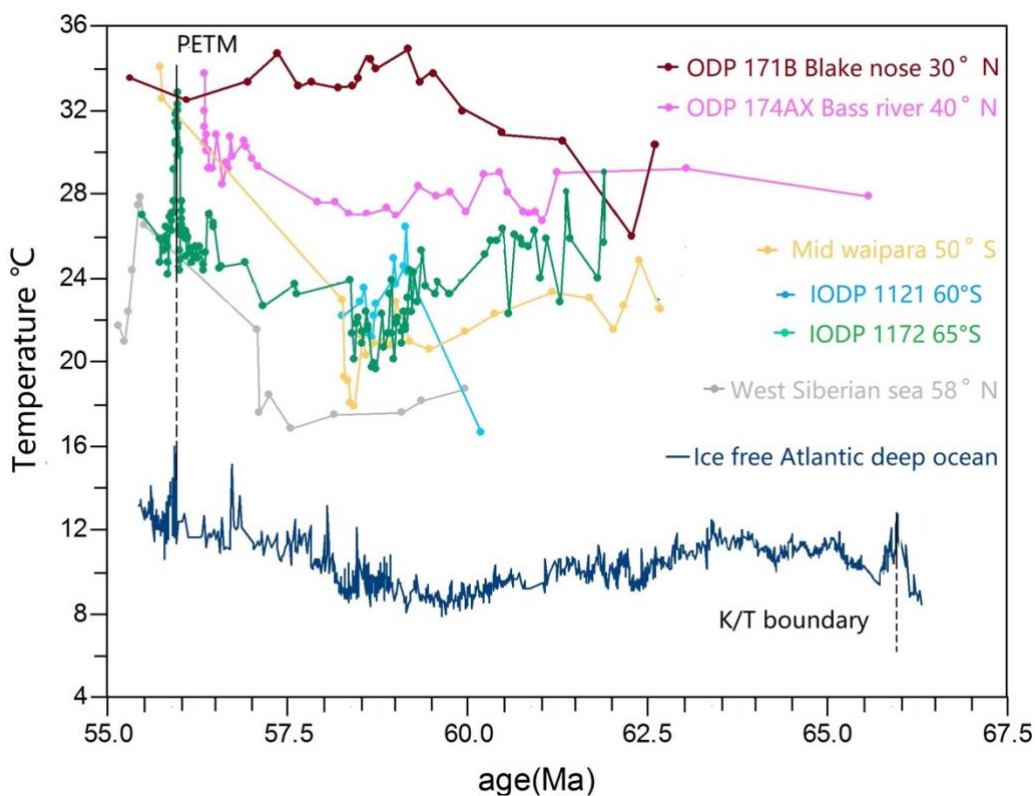


Figure 15 Compilation of TEX$_{86}^{H}$ -based SST records from several sites: ODP 171B (Cramwinckel., 2014), ODP 174AX (this study and Sluijs et al., 2007), mid waipara (Hollis et al., 2014), IODP 1172 (Bijl, personal communication), west Siberian sea (Frieling et al., 2014), and ice free deep Atlantic ocean (Westerhold et al., 2011) Plotted against age (Ma), calibrated to GTS 2012

## 5.4 Paleocene environment reconstruction

### 5.4.1 Paleocene sea level

The reconstruction of Paleocene sea level fluctuation combining temperature reconstruction offer better insights of the glacio-eustatic change in mid-Paleocene and a methane distablization event in LDE. The continental glaciation can influence the sea level by the removal of water mass while temperature influence it through thermal expansion. Furthermore, a regression can decrease hydrostatic pressure on slopes which can destabilize methane hydrates and vice-versa (Jones et al., 2010). Consequently, a positive feedback between temperature and greenhouse gas release can be caused but can also be constrained by thermal expansion. According to some former studies on Cenozoic sea level history, there was a long-term regression-transgression cycle during the Paleocene and the sea level was 40-200 meters above present (Haq et al., 1987; Miller et al., 1997; Müller et al., 2008). However, several sequences have been found by this study and long-term transgression in the North Sea basin and New Jersey shelf is interpreted to be synchronous.
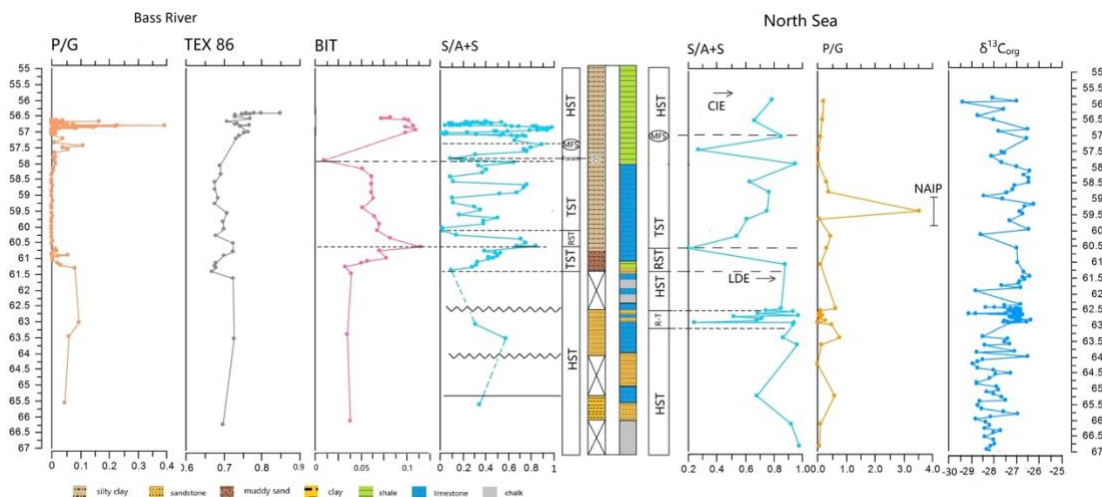


Figure 16 Compilation of Paleocene sea level fluctuation, paleo-prodcutivity from Bass River and North Sea basin against age and available organic geochemistry proxies. Calibrated to GTS 2012

During the early Danian stage in the North Sea basin, S/A index is relatively stable, maintaining 0.8 in 66-63Ma. An abrupt decrease and recovery follows the stable stage, spaning 0.45 Myr. This interval represents a high sedimentation rate, which is contributed by not-sampled turbidite sands. This S/A index reversal suggests a rapid regression-transgression cycle from 62.95Ma to 62.5Ma. The sudden radical decrease occurs at 8736ft (62.92Ma) but it is not accompanied by a sharp lithological transition, and wt.% of carbonate is stable.

The second regression-transgression cycle starts with a decrease at 8617ft (61.89Ma). After the regression, the S/A index enters a long-term increase, lasting ~3.65Myr.

However, a solitary sample (8550.5ft, 57.5Ma) with a S/A drop from 0.8 to 0.27 can be regarded as a third cycle reluctantly. Sample 8508ft indicates the minima of CIE and the influx of *Apectodinuim* spp. This is interpreted as a highstand systems tract (HST) preceding a maximum flooding surface (MFS) in early PETM (Powell et al., 1996; Sluijs et al., 2008; Kender et al., 2012). The sea level rise after the cool period can be caused by the melting of ice sheet (Dutton et al., 2015)

At Bass River, dinocyst assemblage is dominated by the abundant and well preserved *Areoligera* cpx and *Spiniferites* cpx, which provide an ideal tool to reconstruct the sea level changes. In the early Paleocene, Danian stage record is interrupted by 2 hiatus, thus the sea level change during the Danian cannot be reconstructed properly. But the hiatus also indicates a low sea level condition. The abrupt regression-transgression cycle found in the North Sea is not present among the limited remaining Danian sediments. Upper to 382.81mbs, the sediments become successive and the fluctuations of S/A index become much more complicated than in the North Sea. However, the long-term S/A changes pattern resembles each other. The regression-transgression cycles occur conformably, which can be interpreted as a regional integral sea level change in the North Atlantic during the Paleocene period (Figure 16). There is a 100kyr difference between 2 sites which can be caused by the artefact of the age model.

At 382.81 mbs, a minimum of S/A index, points to a lowest sea level at 61.3Ma and the onset of a long-term transgression until 374.40 mbs (57.57Ma). Within this interval, there are numerous short-term variations, but the S/A index is in an uptrend in general. The same interval is also marked by decreasing glauconite until a peak of foraminiferal abundances at 374.90 mbs that separates the TST from HST (Cramer et al., 1999). Hence, both palynological and lithological evidences convince a transgression. This transgression ceases by a macrofossils abundant layer at 374.90 mbs and this is interpreted as an MFS (Cramer et al., 1999). However, the S/A index is at the lowest level (0.1) at this depth and increases dramatically to 0.8 at 374.40 mbs. This discrepancy between dinoflagellates and foraminifer records was not noticed in previous studies (e.g. Sluijs et al., 2008; Cramer et al., 1999).

Although the BIT values are notably low, they can still reveal reproducible fluctuations. Interestingly, comparing BIT with S/A index, the coupling change pattern can be contradictory. From 61.3Ma to 60.44Ma, BIT increased together with S/A increase, which implies that there was more terrestrial input when the sea level is higher. This site is not in the vicinity of riverine input, the hinterland was relatively dry, BIT values are too low to be used as an indicator for sea level at this location. In this case, we should beware BIT cannot always be applied in sea level estimation. BIT proxy mainly indicates the distance to the coast (Hopmans et al., 2004) and sea level is a different concept from coastal distance (BIT) moreover the bias of BIT can be caused by river runoff and variations in continental shelf. However, BIT results also reflect the 2.7 million years long transgression. Terrestrial input reduced gradually from 60.45Ma to 57.92Ma (379.74-373.52mbs) and remained relatively steady during the S/A

fluctuating period. This implies that the coast moved farther to site. It should be noted that S/A index maximun and BIT minimum are not precisely corresponding. For example, in the long-term transgression discussed above, the peak of BIT at 379.74 mbs locates at the peak of S/A index, preceding the S/A index minimum at 379.08 mbs. The different sampling resolution of palynological and organic geochemical analysis can cause such an uncertainty. More likely, the respective responding times of dinocyst assemblage and terrestrially derived branched tetraether lipids to sea level changes are different. Transportation and taphonomy processes should be considered as well.

The interval upper to 374.90 mbs till the onset of CIE has been studied by Sluijs et al. (2008) and Van De Wal. (2011). Based on dinocyst assemblage and BIT results, the site at Bass River indicates that significant sea level rise preceded the CIE, while an MFS seperates TST and HST within the PETM on a global scale (Sluijs et al., 2008). Additionally, 100 kyr short eccentricity cycles also contributed to the climate change in late Paleocene and PETM as maximums of eccentricity coincided high sea level intervals (Van Der Wal., 2011).

5.4.2 Coupling of sea level and temperature and potential methane hydrates dissociation

At Bass River, the correspondence relationship between *Spiniferites* cpx and TEX$_{86}$ found in CCA analysis turns out to be the coupling of sea level and temperature. The long-term transgression lies within the cool mid-Paleocene interval. Although GDGTs derived SST and S/A index at Bass River evolved almost identically against time, there some mismatch occurred as well. For instance, at around 61Ma, the clear S/A reversal trend happened prior to TEX$_{86}$ reversal and the sea level rise also started earlier than the PETM warming (Sluijs et al., 2008). S/A index is generally identical in trend to TEX$_{86}$ including during the long-term transgression. It should be noted that there are 3 S/A peaks within the transgression which lies in the cool period. The SSTs records that locates at the S/A peaks increased about 2°C. This proves that the thermal expansion of sea water sometimes is insufficient to explain the rise of sea level. In addition, S/A index is characterized by the ecology of relevant dinoflagellates genera. The paleobathymetry can be changed by marginal ocean basin reformation while the sea level remains steady (Guasti et al., 2005). Overall, the abrupt S/A index rises relative to the cool period in mid-Paleocene suggests contributions from not only low amplitude temperature fluctuations but also other mechanisms such as continental shelf reform and ocean basin volume decrease (Dick and Zhou, 2014).

If the S/A index-temperature relation is applied to North Sea basin records, some possibilities of the carbon cycle in latest Danian event can be revealed. Some former studies on foraminifera assemblages indicate that there was a rapid sea level fall and rise across LDE (Sprong et al., 2012, 2011) but some other studies indicate a sea level rise during LDE onset (Schulte et al., 2013). In this study, although there is no direct dinocyst assemblage evidence, the preservation of turbidites and relative high S/A trend indicate that LDE happened when the sea level was relative high opposite to the records

by Sprong et al. (2013). Thus, the methane hydrates release was probably due to bottom water temperature exceeding its preservation threshold. Moreover, this study also reveals a phase of anoxic concurrent to sea-level rise and warming as the sandy LDE turbidites sample is overlapped by a thin layer of black shale.

5.4.3 Paleo-productivity and palynological events

Paleoproductivity is reconstructed by P/G index in this study. At Bass River, P-cysts were very barely present in mid and late Paleocene, which suggests an oligotrophic surface water regime. Terrestrial polymorphs are also absent. Combining with BIT results, the paleo-productivity and terrestrial input were very low throughout Paleocene. In the early Paleocene samples, (383.18, 383.43, 383.87 mbs), P/G ration can reach 0.05 and mainly contributed by *Palaeoperidinium pyrophorum*. However, in late Paleocene, a first P/G peak (0.1) occurred at 374 mbs together with a sudden presence of abundant pyritized diatoms (Van Der Wal, 2011). The second but major peak (0.3) at 364 mbs. Both of these two P-cyst peaks mainly contain *Cerodinium Senegalinium* and *Deflandea* genera. The occurrence of such dinoflagellates suggests low salinity and high nutrient supply. The P/G peaks also coincide with temperature increase. Thus, temperature can be considered as a limit of eutrophication at this site. Nutrients level was enhanced during relative warm periods. Low salinity and nutrients supply were intensified during the warming period. The mechanisms of these phenomena can be various. The increase of BIT concomitant with P/G ratio indicates more terrigenous material input during late Paleocene warming. The decrease in BIT is caused by brGDGTs increase and together with iGDGTs increase. As more extreme climate events will happen in extreme greenhouse world based on modeling and simulation (Sriver and Huber, 2007; Emanuel, 2005; Emanuel et al., 2004; Easterling et al., 2000). Therefore, an intensification of storms which can not only agitate deeper nutrient-rich waters to the photic zone but also enhance precipitation. This eutrophication pattern was also found at Bass River during the PETM warming (Sluijs et al., 2009). Therefore, the cool mid-Paleocene at Bass river experienced a relatively less humid climate and a reduction of terrestrial input from surrounding lands.

Peridinioid cysts are much more abundant in both amount and taxonomy in the North Sea basin core 22/10a-5. P/G ration can even reach 0.8 due to *P. pyrophorum* acme. In general, P/G ration varies in the same trend as S/A ratio not only during the rapid regression-transgression cycle but also in the long-term transgression. If sea level-temperature relation is applied to the North Sea basin, its paleo-productivity is also correlated by climate warming. Furthermore, an increase of C/N ratio and kaolinite contributon of 22/10a-4 suggests that the reduction of sea water salinity and eutrophication were associated with increased terrestrial input (Kender et al., 2014). The percentage of P-cyst increased gradually from 8% to 20% at the CIE sample in the core 22/10a-5. In the core 22/10a-4, P-cyst also reached 20% at the onset of PETM CIE (Kender et al., 2012). Thus, the CIE recognized at 8508.8ft is very likely to be the PETM event.

However, there is an anomaly around 59.54Ma (8586ft), which is characterized by a sudden acme of *P.pyrophorum* and abundant bisaccate *Pinus* pollens. This event locates in the sea level gradual rising stage. A similar acme was also known from the Selandian in the Viborg 1 borehole, Denmark (Heilmann-Clausen, 1985). Such a *P.pyrophorum* acme was interpreted as a regional cold-water pulse by Willumsen and Vajda (2010). Since this sample is almost monotypic, S/A index may be not applicable. According to the large amount of *P.pyrophorum* and bisaccate pollens, this sample more likely indicates a short term sea level rise. As the main volcanism basalt flood of NAIP was active from 60.5 Ma to 54.5 Ma in north Atlantic Ocean (Jolley and Bell, 2002), this sea level rise can be interpreted as due to either tectonic uplift possibly from a surrounding lava intrusion (Kender et al., 2012). It can be explained as increased precipitation and fluvial runoff possibly from an enhanced hydrologic cycle as because the preferential habitation of *P.pyrophorum* is associated with fresh cold water pulse. Bisaccate pollens are mainly produced by a variety of lowland swamp coniferous plants in the north Europe and can be transported by wind (Boulter and Manum 1989; Greenwood and Basinger, 1993; Jolley and Whitham 2004; Jolley and Morton 2007). However, in the overlying sample, the bisaccate pollens were rapidly replaced by trilete spores. This rapid succession in lowland swamp vegetation from coniferous-dominated communities to generalist fern spores would be consistent with flooding driven coastal swamp plains due to local sea level rise and the increase of temperature and precipitation (Kender et al., 2014). There are also seasonal temperature and precipitation prior to the CIE reconstructed by vegetation shift at the North Sea (Eldrett et al., 2014).

# 6. Conclusion:

This study improved our cognition on sea level history and temperature evolution of the enigmatic mid-Paleocene, in addition, established a framework of biostratigraphy in the North Sea basin. Through the evidence in mid latitude Bass River and high latitude North Sea basin, although the questions posed are not completely answered, the discoveries at these two sites can reveal some new insights of the presence of Antarctica ice sheet, relevant climate change.

Based on the temperature reconstruction by $TEX_{86}^{H}$ calibration, the Bass River core revealed that the 2℃ cooling of mid-Paleocene consists of 2 stage, around 61 and 59Ma respectively. Compiling with the SSTs records from both hemispheres in different latitudes, a significant meridional temperature gradient reduction and amplitude difference during the cooling was found in the south hemisphere. The temperature at 50°, 60°, 65° S were all around 21℃. Therefore, the presence of ice sheet in the Antarctica can be a plausible reason for such an unbalanced thermal distribution. Temperature increase can enhance the carbon cycle and cause a positive feedback. The sandy turbidity, barren dinoflagellates and negative $\delta^{13}C_{org}$ from the North Sea basin suggest that there is a methane hydrates dissociation caused by sea water temperature increase rather than hydraulic pressure change in the LDE.

There is a strong correlation between the palynological proxy S/A which can indicate sea level and SSTs derived from GDGTs. However, the different S/A response amplitudes to temperature change imply that thermal expansion is not the only cause of sea level rise, ocean basin volume change and continental reformation should be considered as well. The mismatches between S/A and BIT may be cautionary for proxies application that different biochemical and sedimentary process may cause a divergence between different proxies.

Paleo-productivity was notably low during the cool period of Paleocene by means of nearly zero P/G dinocysts ratio. Productivity would increase during the warming or sea level rising stage, thus verifying the hypothesis that there are more precipitation and extreme weathers in a warming world. Local tectonic activity such NAIP would attribute to short term sea level change as well and cause sudden dinoflagellates acme and even on land vegetation succession.

## 7. Outlook

Although a biostratigraphy and age model have been established for the North Sea basin core 22/10a-5, there are still some uncertainties of the start and end datum of the Paleocene. The occurrence of *Apectodinium* sp. and *Palynodinium grallator / Spongodinium* sp. cannot really constrain the ends of Paleocene. Thus, some more palynological analyses on the deeper and shallower samples can improve the stratigraphy framework.

As the mismatches or lags between different proxies such as S/A, BIT and $TEX_{86}$ were found in this study, the synthetical application of these proxies became suspicious. Therefore, a higher sampling resolution around the proxy reversal depth would help figure out the sequence and mechanism of different biochemical proxies responses to the environment change and the interaction between each other. Additionally, C:N atomic ratio can supplement the interpretation of terrestrial input change.

Terrestrial palynomorphs were not analyzed systematically in this study. The major pollen and spore replacement that was found associated with local sea level fall and NAIP activity by a rough counting would warrant a more detailed analysis on terrestrial palynomorphs including plant cuticula and fresh water algae. This would reflect the vegetation shift on surrounding landmasses., consequently shed a light on sea level change and precipitation from another perspective.

Although from the temperature distribution pattern in the cool mid-Paleocene, at least a short scale of ice sheet was inferred to be present in the Antarctica, an evidence about atmospheric $CO_2$ is still lacking.

## Acknowledgements

It is said that: a fungus never knows the start and the end of a month, a cicada never knows spring and autumn (Zhuangzi, 476-221BC). It is an honor and fortunate to be a human that we can have a chance to peek at earth's history through a drilling hole. I believe that someday in the far future, the resolution of human beings will be recorded on the earth as well.

# References

Bernaola, G., Baceta, J. I., Orue-Etxebarria, X., Alegret, L., Martín-Rubio, M., Arostegui, J., & Dinarès-Turell, J. (2007). Evidence of an abrupt environmental disruption during the mid-Paleocene biotic event (Zumaia section, western Pyrenees). *Geological Society of America Bulletin*, *119*(7-8), 785-795.

Bijl, P. K., Schouten, S., Sluijs, A., Reichart, G. J., Zachos, J. C., & Brinkhuis, H. (2009). Early Palaeogene temperature evolution of the southwest Pacific Ocean. *Nature,* 461(7265), 776.

Bijl, P. K., Bendle, J. A., Bohaty, S. M., Pross, J., Schouten, S., Tauxe, L., ... & Sluijs, A. (2013a). Eocene cooling linked to early flow across the Tasmanian Gateway. *Proceedings of the National Academy of Sciences*, 110(24), 9645-9650.

Bijl, P. K., Sluijs, A., & Brinkhuis, H. (2013b). A magneto-and chemostratigraphically calibrated dinoflagellate cyst zonation of the early Palaeogene South Pacific Ocean. *Earth-Science Reviews*, *124*, 1-31.

Boulter, M. C., & Manum, S. B. (1989). The Brito-Arctic igneous province flora around the Paleocene/Eocene boundary. In *Proceedings of the Ocean Drilling Program, Scientific Results* (Vol. 104, pp. 663-680).

Bornemann, A., Schulte, P., Sprong, J., Steurbaut, E., Youssef, M., & Speijer, R. P. (2009). Latest Danian carbon isotope anomaly and associated environmental change in the southern Tethys (Nile Basin, Egypt). *Journal of the Geological Society*, *166*(6), 1135-1142.

Brinkhuis, H. (1994). Late Eocene to Early Oligocene dinoflagellate cysts from the Priabonian type-area (Northeast Italy): biostratigraphy and paleoenvironmental interpretation. *Palaeogeography, Palaeoclimatology, Palaeoecology*, *107*(1-2), 121-163.

Costa, L. I., Davey, R. J., & Powell, A. J. (1992). A stratigraphic index of dinoflagellate cysts. *British Micropalaeontological Society Series*, 99-153.

Costa, L. I., & Davey, R. J. (1992). Dinoflagellate cysts of the Cretaceous System. In *A stratigraphic index of dinoflagellate cysts* (pp. 99-153). Springer Netherlands.

Contreras, L., Pross, J., Bijl, P. K., O'Hara, R. B., Raine, J. I., Sluijs, A., & Brinkhuis, H. (2014). Southern high-latitude terrestrial climate change during the Palaeocene–Eocene derived from a marine pollen record (ODP Site 1172, East Tasman Plateau). *Climate of the Past*, *10*(4), 1401-1420.

Cramer, B. S., Aubry, M. P., Miller, K. G., Olsson, R. K., Wright, J. D., & Kent, D. V. (1999). An exceptional chronologic, isotopic, and clay mineralogic record of the latest Paleocene thermal maximum, Bass River, NJ, ODP 174AX. *Bulletin de la Société géologique de France*, *170*(6), 883-897.

Cramwinckel, M. (2014). Low-latitude climate evolution during the Paleocene a biogeochemical and palynological study of ODP Leg 171B. *Utrecht University master thesis*

Cramwinckel, M. J., Huber, M., Kocken, I. J., Agnini, C., Bijl, P. K., Bohaty, S. M., ... & Peterse, F. (2018). Synchronous tropical and polar temperature evolution in the Eocene. *Nature*.

Damsté, J. S. S., Schouten, S., Hopmans, E. C., van Duin, A. C., & Geenevasen, J. A. (2002). Crenarchaeol the characteristic core glycerol dibiphytanyl glycerol tetraether membrane lipid of cosmopolitan pelagic crenarchaeota. *Journal of Lipid Research*, *43*(10), 1641-1651.

Dick, H. J., & Zhou, H. (2015). Ocean rises are products of variable mantle composition, temperature and focused melting. *Nature Geoscience*, *8*(1), 68.

Duarte, C. M., & Cebrián, J. (1996). The fate of marine autotrophic production. *Limnology and Oceanography*, *41*(8), 1758-1766.

Dutton, A., Carlson, A. E., Long, A. J., Milne, G. A., Clark, P. U., DeConto, R., ... & Raymo, M. E. (2015). Sea-level rise due to polar ice-sheet mass loss during past warm periods. *science*, *349*(6244), aaa4019.

Easterling, D. R., Evans, J. L., Groisman, P. Y., Karl, T. R., Kunkel, K. E., & Ambenje, P. (2000). Observed variability and trends in extreme climate events: a brief review. *Bulletin of the American Meteorological Society*, *81*(3), 417-426.

Eldrett, J. S., Greenwood, D. R., Polling, M., Brinkhuis, H., & Sluijs, A. (2014). A seasonality trigger for carbon injection at the Paleocene–Eocene Thermal Maximum. *Climate of the Past*, *10*(2), 759-769.

Ellegaard, M. (2000). Variations in dinoflagellate cyst morphology under conditions of changing salinity during the last 2000 years in the Limfjord, Denmark. *Review of Palaeobotany and Palynology*, *109*(1), 65-81.

Emanuel, K., DesAutels, C., Holloway, C., & Korty, R. (2004). Environmental control of tropical cyclone intensity. *Journal of the atmospheric sciences*, *61*(7), 843-858.

Emanuel, K. (2005). Increasing destructiveness of tropical cyclones over the past 30 years. *Nature*, *436*(7051), 686.

Emiliani, C. (1955). Pleistocene temperatures. The Journal of Geology, 63(6), 538-578.

Erez, J., & Luz, B. (1983). Experimental paleotemperature equation for planktonic foraminifera. *Geochimica et Cosmochimica Acta*, *47*(6), 1025-1031.

Evitt, W. R. (1985). *Sporopollenin dinoflagellate cysts: their morphology and interpretation*. Amer Assn of Stratigraphic.

Fedorov, A. V., Burls, N. J., Lawrence, K. T., & Peterson, L. C. (2015). Tightly linked zonal and meridional sea surface temperature gradients over the past five million years. *Nature Geoscience*, *8*(12), 975.

Fedorov, A. V., Brierley, C. M., Lawrence, K. T., Liu, Z., Dekens, P. S., & Ravelo, A. C. (2013). Patterns and mechanisms of early Pliocene warmth. *Nature*, *496*(7443), 43.

Fensome, R. A., Taylor, F. J. R., Norris, G., & Sarjeant, W. AS, WHARTON, DI & WILLIAMS, GL (1993): A classification of living and fossil dinoflagellates. *Micropaleontology, Special Publication*, *7*.

Fensome, R. A., & Williams, G. L. (2004). *The Lentin and Williams index of fossil dinoflagellages*. American Association of Stratigraphic Palynologists Foundation.

Firth, J. V., & Clark, D. L. (1998). An early Maastrichtian organic-walled phytoplankton cyst assemblage from an organic-rich black mud in Core Fl-533, Alpha Ridge: evidence for upwelling conditions in the Cretaceous Arctic Ocean. *Marine Micropaleontology*, *34*(1-2), 1-27.

Gradstein, F. M., Ogg, J. G., Schmitz, M., & Ogg, G. (Eds.). (2012). *The geologic time scale 2012*. elsevier.

Greenwood, D. R., & Basinger, J. F. (1993). Stratigraphy and floristics of Eocene swamp forests from Axel Heiberg Island, Canadian Arctic Archipelago. *Canadian Journal of Earth Sciences*, *30*(9), 1914-1923.

Guasti, E., Kouwenhoven, T. J., Brinkhuis, H., & Speijer, R. P. (2005). Paleocene sea-level and productivity changes at the southern Tethyan margin (El Kef, Tunisia). *Marine Micropaleontology*, *55*(1-2), 1-17.

Heilmann-Clausen, C. (1985). *Dinoflagellate stratigraphy of the uppermost Danian to Ypresian in the Viborg 1 borehole, central Jylland, Denmark* (No. 10). Danmarks geologiske undersøgelse.

Haq, B. U., Hardenbol, J. A. N., & Vail, P. R. (1987). Chronology of fluctuating sea levels since the Triassic. *Science*, *235*(4793), 1156-1167.

Hammer, Ø., Harper, D. A. T., & Ryan, P. D. (2001). Paleontological statistics software: package for education and data analysis. *Palaeontologia Electronica*, (4).

Hedges, J. I., & Keil, R. G. (1995). Sedimentary organic matter preservation: an assessment and speculative synthesis. *Marine chemistry*, *49*(2-3), 81-115.

Hinrichs, K. U., Hayes, J. M., Sylva, S. P., Brewer, P. G., & DeLong, E. F. (1999). Methane-consuming archaebacteria in marine sediments. *Nature*, *398*(6730), 802.

Hollis, C. J., Taylor, K. W., Handley, L., Pancost, R. D., Huber, M., Creech, J. B., ... & Gibbs, S. (2012). Early Paleogene temperature history of the Southwest Pacific Ocean: Reconciling proxies and models. *Earth and Planetary Science Letters*, *349*, 53-66.

Hollis, C. J., Tayler, M. J., Andrew, B., Taylor, K. W., Lurcock, P., Bijl, P. K., ... & Huber, M. (2014). Organic-rich sedimentation in the South Pacific Ocean associated with Late Paleocene climatic cooling. *Earth-Science Reviews*, *134*, 81-97.

Hopmans, E. C., Schouten, S., & Sinninghe Damsté, J. S. (2016). The effect of improved chromatography on GDGT-based palaeoproxies. *Organic Geochemistry*, *93*, 1–6.

Jan Du Chêne, R. E. (1988). Étude systématique des kystes de dinoflagellés de la Formation des Madeleines (Danien du Sénégal). *Cahiers de micropaléontologie, Nouvelle série*, *2*, 147-174.

Jolley, D. W., & Whitham, A. G. (2004). A stratigraphical and palaeoenvironmental analysis of the sub-basaltic Palaeogene sediments of East Greenland. *Petroleum Geoscience*, *10*(1), 53-60.

Jolley, D. W., & Morton, A. C. (2007). Understanding basin sedimentary provenance: evidence from allied phytogeographic and heavy mineral analysis of the Palaeocene of the NE Atlantic. *Journal of the Geological Society*, *164*(3), 553-563.

Jolly, R. J., & Lonergan, L. (2002). Mechanisms and controls on the formation of sand intrusions. *Journal of the Geological Society*, *159*(5), 605-617.

Jones, T. D., Ridgwell, A., Lunt, D. J., Maslin, M. A., Schmidt, D. N., & Valdes, P. J. (2010). A Palaeogene perspective on climate sensitivity and methane hydrate instability. *Philosophical Transactions of the Royal Society of London A: Mathematical, Physical and Engineering Sciences*, *368*(1919), 2395-2415.

Juggins, S. (2003). C2 User guide. *Software for ecological and palaeoecological data analysis and visualisation. University of Newcastle, Newcastle upon Tyne*, *69*.

Kim, J. H., Van der Meer, J., Schouten, S., Helmke, P., Willmott, V., Sangiorgi, F., ... & Damsté, J. S. S. (2010). New indices and calibrations derived from the distribution of crenarchaeal isoprenoid tetraether lipids: Implications for past sea surface temperature reconstructions. *Geochimica et Cosmochimica Acta*, 74(16), 4639-4654.

Komar, N., Zeebe, R. E., & Dickens, G. R. (2013). Understanding long-term carbon cycle trends: The late Paleocene through the early Eocene. *Paleoceanography*, *28*(4), 650-662.

Knox, R. O. B. (1998). The tectonic and volcanic history of the North Atlantic region during the Paleocene-Eocene trasition: implications for NW European and global biotic events. *Late Paleocene-Early Eocene Climatic and Biotic Events in the Marine and Terrestrial Records*, 91-102.

Kvenvolden, K. A. (1999). Potential effects of gas hydrate on human welfare. *Proceedings of the National Academy of Sciences*, *96*(7), 3420-3426.

Littler, K., Röhl, U., Westerhold, T., & Zachos, J. C. (2014). A high-resolution benthic stable-isotope record for the South Atlantic: Implications for orbital-scale changes in Late Paleocene–Early Eocene climate and carbon cycling. *Earth and Planetary Science Letters*, *401*, 18-30.

Liu, C., Browning, J. V., Miller, K. G., and Olsson, R. K.: Paleocene benthic foraminiferal biofacies and sequence stratigraphy, Island Beach borehole, New Jersey, in: Proceedings of the Ocean Drilling Program, Scientific Results, 150X, edited by: Miller, K. G., and Snyder, S. W., Ocean Drilling Program, College Station, TX, 267–375, 1997.

Miller, K. G., Sugarman, P. J., Browning, J. V., et al.: Proceedings of the Ocean Drilling Program, Initial Reports 174AX. doi:10.2973/odp.proc.ir.174ax.1998, Ocean Drilling Program, College Station, TX, 1998.

Mudge, D. C., & Bujak, J. P. (1996). Palaeocene biostratigraphy and sequence stratigraphy of the UK central North Sea. *Marine and Petroleum Geology*, *13*(3), 295-312.

Müller, R. D., Sdrolias, M., Gaina, C., Steinberger, B., & Heine, C. (2008). Long-term sea-level fluctuations driven by ocean basin dynamics. *science*, *319*(5868), 1357-1362.

Pagani, M., Caldeira, K., Archer, D., & Zachos, J. C. (2006). An ancient carbon mystery. *SCIENCE-NEW YORK THEN WASHINGTON-*, *314*(5805), 1556.

Pancost, R. D., Hopmans, E. C., & Damsté, J. S. (2001). Archaeal lipids in Mediterranean cold seeps: molecular proxies for anaerobic methane oxidation. *Geochimica et Cosmochimica Acta*, *65*(10), 1611-1627.

Pearson, P. N., & Palmer, M. R. (2000). Atmospheric carbon dioxide concentrations over the past 60 million years. *Nature*, *406*(6797), 695.

Powell, A. J., Brinkhuis, H., & Bujak, J. P. (1996). Upper Paleocene-Lower Eocene dinoflagellate cyst sequence biostratigraphy of southeast England. *Geological Society, London, Special Publications*, *101*(1), 145-183.

Prauss, M. (2001). Sea-level changes and organic-walled phytoplankton response in a Late Albian epicontinental setting, Lower Saxony basin, NW Germany. *Palaeogeography, Palaeoclimatology, Palaeoecology*, *174*(1-3), 221-249.

Pross, J., & Brinkhuis, H. (2005). Organic-walled dinoflagellate cysts as paleoenvironmental indicators in the Paleogene; a synopsis of concepts. *Paläontologische Zeitschrift*, *79*(1), 53-59.

Rahmstorf, S., & Coumou, D. (2011). Increase of extreme events in a warming world. *Proceedings of the National Academy of Sciences*, *108*(44), 17905-17909.

Reichart, G. J., & Brinkhuis, H. (2003). Late Quaternary Protoperidinium cysts as indicators of paleoproductivity in the northern Arabian Sea. *Marine Micropaleontology*, *49*(4), 303-315.

Royer, D. L., & Beerling, D. J. (2011, December). Convergent Cenozoic CO2 history. In *AGU Fall Meeting Abstracts*.

Schouten, S., Hopmans, E. C., Schefuß, E., & Damste, J. S. S. (2002). Distributional variations in marine crenarchaeotal membrane lipids: a new tool for reconstructing ancient sea water temperatures?. *Earth and Planetary Science Letters*, 204(1-2), 265-274.

Schouten, S., Woltering, M., Rijpstra, W. I. C., Sluijs, A., Brinkhuis, H., & Damsté, J. S. S. (2007). The Paleocene–Eocene carbon isotope excursion in higher plant organic matter: differential fractionation of angiosperms and conifers in the Arctic. *Earth and Planetary Science Letters*, *258*(3-4), 581-592.

Schulte, P., Schwark, L., Stassen, P., Kouwenhoven, T. J., Bornemann, A., & Speijer, R. P. (2013). Black shale formation during the Latest Danian Event and the Paleocene–Eocene Thermal Maximum in central Egypt: Two of a kind?. *Palaeogeography, palaeoclimatology, palaeoecology*, *371*, 9-25.

Sluijs, A., Pross, J., & Brinkhuis, H. (2005). From greenhouse to icehouse; organic-walled dinoflagellate cysts as paleoenvironmental indicators in the Paleogene. *Earth-Science Reviews*, *68*(3-4), 281-315.

Sluijs, A., Brinkhuis, H., Schouten, S., Bohaty, S. M., John, C. M., Zachos, J. C., ... & Dickens, G. R. (2007). Environmental precursors to rapid light carbon injection at the Palaeocene/Eocene boundary. *Nature*, *450*(7173), 1218.

Sluijs, A., Brinkhuis, H., Crouch, E. M., John, C. M., Handley, L., Munsterman, D., ... & Pancost, R. D. (2008). Eustatic variations during the Paleocene-Eocene greenhouse world. *Paleoceanography*, *23*(4).

Sluijs, A., & Brinkhuis, H. (2009). A dynamic climate and ecosystem state during the Paleocene-Eocene Thermal Maximum: inferences from dinoflagellate cyst assemblages on the New Jersey Shelf. *Biogeosciences*, *6*(8).

Speijer, R. P. (2003). Danian-Selandian sea-level change and biotic excursion on the southern Tethyan margin (Egypt). *SPECIAL PAPERS-GEOLOGICAL SOCIETY OF AMERICA*, 275-290.

Sprong, J., Youssef, M. A., Bornemann, A., Schulte, P., Steurbaut, E., Stassen, P., ... & Speijer, R. P. (2011). A multi-proxy record of the latest Danian Event at Gebel Qreiya, Eastern Desert, Egypt. *Journal of Micropalaeontology*, *30*(2), 167-182.

Sprong, J., Kouwenhoven, T. J., Bornemann, A., Schulte, P., Stassen, P., Steurbaut, E., ... & Speijer, R. P. (2012). Characterization of the Latest Danian Event by means of benthic foraminiferal assemblages along a depth transect at the southern Tethyan margin (Nile Basin, Egypt). *Marine Micropaleontology*, *86*, 15-31.

Sriver, R. L., & Huber, M. (2007). Observational evidence for an ocean heat pump induced by tropical cyclones. *Nature*, *447*(7144), 577.

Van de Wal, S. (2011). Paleocene orbitally forced climate and carbon cycle variations on the New Jersey shelf. *Utrecht University master thesis*

Van Hinsbergen, D. J., de Groot, L. V., van Schaik, S. J., Spakman, W., Bijl, P. K., Sluijs, A., ... & Brinkhuis, H. (2015). A paleolatitude calculator for paleoclimate studies. *PloS one*, 10(6), e0126946.

Vellekoop, J., Smit, J., van de Schootbrugge, B., Weijers, J. W., Galeotti, S., Damste, J. S. S., & Brinkhuis, H. (2015). Palynological evidence for prolonged cooling along the Tunisian continental shelf following the K–Pg boundary impact. *Palaeogeography, palaeoclimatology, palaeoecology*, *426*, 216-228.

Vellekoop, J., Esmeray-Senlet, S., Miller, K. G., Browning, J. V., Sluijs, A., van de Schootbrugge, B., ... & Brinkhuis, H. (2016). Evidence for Cretaceous-Paleogene boundary bolide "impact winter" conditions from New Jersey, USA. *Geology*, *44*(8), 619-622.

Westerhold, T., Röhl, U., Raffi, I., Fornaciari, E., Monechi, S., Reale, V., ... & Evans, H. F. (2008). Astronomical calibration of the Paleocene time. *Palaeogeography, Palaeoclimatology, Palaeoecology*, *257*(4), 377-403.

Westerhold, T., Röhl, U., Donner, B., McCarren, H. K., & Zachos, J. C. (2011). A complete high-resolution Paleocene benthic stable isotope record for the central Pacific (ODP Site 1209). *Paleoceanography*, *26*(2).

Willumsen, P., & Vajda, V. (2010, May). Ecosystems response and restitution time across the K/Pg boundary transition at high-latitudes, Southern Hemisphere, New Zealand-a palynological approach. In *EGU General Assembly Conference Abstracts* (Vol. 12, p. 11379).

Zachos, J. C., Arthur, M. A., & Dean, W. E. (1989). Geochemical evidence for suppression of pelagic marine productivity at the Cretaceous/Tertiary boundary. *Nature*, *337*(6202), 61.

Zachos, J. C., Dickens, G. R., & Zeebe, R. E. (2008). An early Cenozoic perspective on greenhouse warming and carbon-cycle dynamics. *Nature*, *451*(7176), 279.

Zachos, J. C., McCarren, H., Murphy, B., Röhl, U., & Westerhold, T. (2010). Tempo and scale of late Paleocene and early Eocene carbon isotope cycles: Implications for the origin of hyperthermals. *Earth and Planetary Science Letters*, *299*(1), 242-249.

Zhang, Y. G., Zhang, C. L., Liu, X. L., Li, L., Hinrichs, K. U., & Noakes, J. E. (2011). Methane Index: a tetraether archaeal lipid biomarker indicator for detecting the instability of marine gas hydrates. *Earth and Planetary Science Letters*, *307*(3), 525-534.

Zhang, Y. G., Pagani, M., Liu, Z., Bohaty, S. M., & DeConto, R. (2013). A 40-million-year history of atmospheric CO2. *Phil. Trans. R. Soc. A*, *371*(2001), 20130096.

Zhang, Y. G., Pagani, M., & Wang, Z. (2016). Ring Index: A new strategy to evaluate the integrity of TEX86 paleothermometry. *Paleoceanography*, *31*(2), 220-232.

**Appendix 1. Systematic palynology**

The different genera, species and groups that were found in the palynological assemblage are listed below. In total, 85 dinocyst taxa were recognized in these two sites. Dinocyst taxonomy follows Fensome and Williams, (2004). Dinoflagellates species are seperated in gonyaulacoid cysts and peridinoid cysts respectively in alphabetical order. Terrestrial palynomorphs and several acritarchs are also presented.

**Dinoflagellate cysts**

**Gonyaulacoid cysts**
*Achilleodinium* sp.(bifomoids) Evitt, 1978
*Achomosphaera alcicornu* (Eisenack 1954b), Davey and Williams 1966a
*Achomosphaera crassipellis / ramulifera* (Deflandre and Cookson, 1955) Stover & Evitt, 1978
*Adnatosphaeridium multispinosum* Williams and Downie, 1966
*Alisocysta circumtabulata* (Drugg, 1967)
*Alisocysta margarita* Quattrochio and Sarjeant, 2003
*Alisocysta reticulata* Quattrochio and Sarjeant, 2003
*Areoligera* sp. Stover and Evitt, 1978
*Areoligera coronata* (O. Wetzel, 1933) Lejeune-Carpentier, 1938
*Areoligera gippingensi*s
**Remark:** A. gippingensis is also named as A. senonensis by some literatures. All the speciemen with basally circular processes were counted as A.gippingensis in the North Sea.
*Areoligera 'horrida'*
*Batiacasphaera cassicula* Wilson 1988
*Caligodinium aceras*
*Chatagiella* sp.
*Cladopyxium saeptum* (Morgenroth, 1968) Stover and Evitt, 1978
*Cleistosphaeridinium placacantum* Davey et al., 1966
*Cleistosphaeridium* sp. Davey et al., 1966
*Cordosphaeridium fibrospinosum* Davey and Williams, 1966
*Cordosphaeridium gracile* (Eisenack, 1954) emend. Davey and Williams, 1966
*Cordosphaeridium inodes* (Klumpp, 1953) Eisenack, 1963; emend. Morgenroth, 1968; emend. Sarjeant, 1981
*Cordosphaeridium* sp.
*Cribroperidinium wetzelii* (Lejeune-Carpentier, 1939) Helenes, 1984
*Dapsilidinium pastielsii* (Davey and Williams, 1966) Bujak et al., 1980

*Diphyes colligerum* (Deflandre and Cookson, 1955) emend. Cookson, 1965; emend. Davey and Williams, 1966; emend. Goodman and Witmer, 1985

*Eatonicysta ursulae*

*Eocladopyxis* sp. Morgenroth, 1966; emend. Stover and Evitt, 1978

*Fibrocyst*a sp. Stover and Evitt, 1978

Fib*rocysta axialis*

*Fibrocysta bipolaris*

*Fibrocysta vectense*

*Florentinia* sp. Davey and Verdier, 1973; emend. Duxbury, 1980

*Florentinia ferox*

*Florentinia rechartii* Sluijs et al., 2009

*Glaphyrocysta divaricata* (Williams and Downie, 1966) Stover and Evitt, 1978

*Glaphyrocysta ordinata* (Williams and Downie, 1966) Stover and Evitt, 1978

*Glaphyrocysta pastielsii* (Deflandre and Cookson, 1955) Stover and Evitt, 1978; emend. Sarjeant, 1986

**Remark:** distinction between different species of Glaphyrocysta based on process forms, following Heilmann-Clausen (1985)

*Glaphyrocysta* sp.

*Hafniasphaera septata* (Cookson and Eisenack, 1967b) Hansen, 1977

*Hystrichokopolma truncatum* Deflandre and Cookson, 1955

*Hystrichokopolma bulbosum* Deflandre and Cookson, 1955

Hystrichosphaeridium tubiferum (Ehrenberg, 1838) Deflandre, 1937; emend. Davey and Williams, 1966

*Hystristogylon coninckii*

*Hystristogylon membraniphora*

*Impagidinium* sp (Wall, 1967) Lentin and Williams, 1981

*Kallosphaeridinium parvum*

*Lingulodinium*

*Meltasphaeridinium sp.*

*Membranosphaer*a

*Oligosphaeridium* sp. (White, 1842) Davey and Williams, 1966

*Operculodinium* sp. Wall, 1967

*Pyxidinopsis ardonensis* Du Chêne, 1988

*Palynodinium grallator*

*Rottnestia borussica*

*Senoniasphaera inornata*

*Spiniferella cornuta*

*Spiniferites pseudofurcatus* (Klumpp, 1953) Sarjeant 1970

Spiniferites ramosus (Ehrenberg 1838, Mantell 1854)

*Spiniferites mirabilis (*Ehrenberg 1838, Mantell 1854)

S*piniferites splendidus* (Ehrenberg 1838, Mantell 1854)

*Spiniferites sp.* (Mantell, 1850 emend. Sarjeant 1970)

*Spongodinium s*p.

T*anyosphaeridium xanthiopyxides* (O. Wetzel, 1933; emend. Morgenroth, 1968)

Stover and Evitt, 1978; emend. Sarjeant, 1985
*Thalassphora delicata*
*Thalassphora inflata*
*Thalassphora pelagica*

**Peridinioid cysts**
*Apectodinium so.*
*Aectodinium augstum*
*Apectodinium homomorphum*
*A. hyperacantha*
*A. quinquelatum*
*Cerodinium diebelii* (Alberti, 1959) Lentin and Williams, 1987
*Cerodinium depressum* (Morgenroth, 1966) Lentin and Williams, 1987
*Cerodinium striatum* (Drugg, 1967) Lentin and Williams, 1987
*Cerodinium speciosum* (Alberti, 1959) Lentin and Williams, 1987
*Deflandrea sp.*
*Deflandrea oesibian*
*Deflandrea phosphate*
*Isabelidinium viborgense* Heilman Clausen ,1985
*Senegalinium* spp. Jain and Millepied, 1973; emend. Stover and Evitt, 1978
*Spinidinium densispinatum* Stanley, 1965
*Paleocystodinium golzowense* Alberti, 1961
*Paleocystodinium lidiae* (Górka, 1963) emend. Davey, 1969
*Palaeoperidinium pyrophorum* (Ehrenberg, 1838) Sarjeant, 1967 emend. Gocht and Netzel, 1976

**Other palynomorphs**
Pyritized diatom
Organic foraminiferal linings
Bissacate pollen
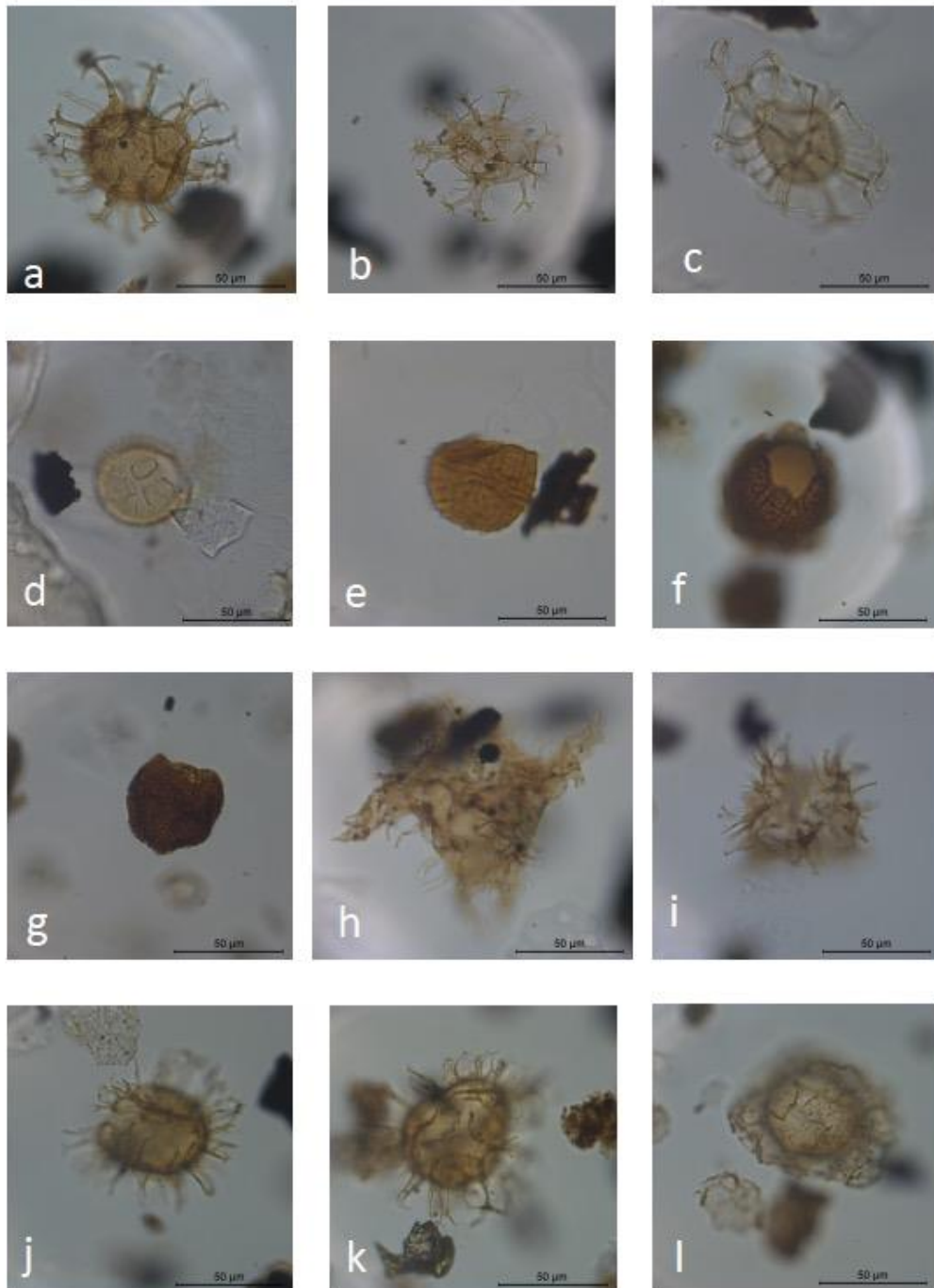Trilete spore
Acritarch

# Appendix 2 plates



**Plate 1.** a: *Achomosphaera alcicornu* NSP11 8575.35ft b: *Achomosphaera ramulifera* 8713.45ft c: *Adnatosphaeridinium robustum* NSP17 8723.8ft d: *Alisocysta circumtabulata* BRP17 1241.05ft e: *Alisocysta margarita* NSP1 8527.5ft f, g: *Alisocysta reticulata* NSP17 8723.8ft h: *Apectodinium augustum* NSP9 8508.5ft i: *Apectodinium homomorphum* NSP9 8508.5ft j,k: *Areoligera gippingensis* 8569.5ft l: *Areoligera 'horrida'* 8601ft
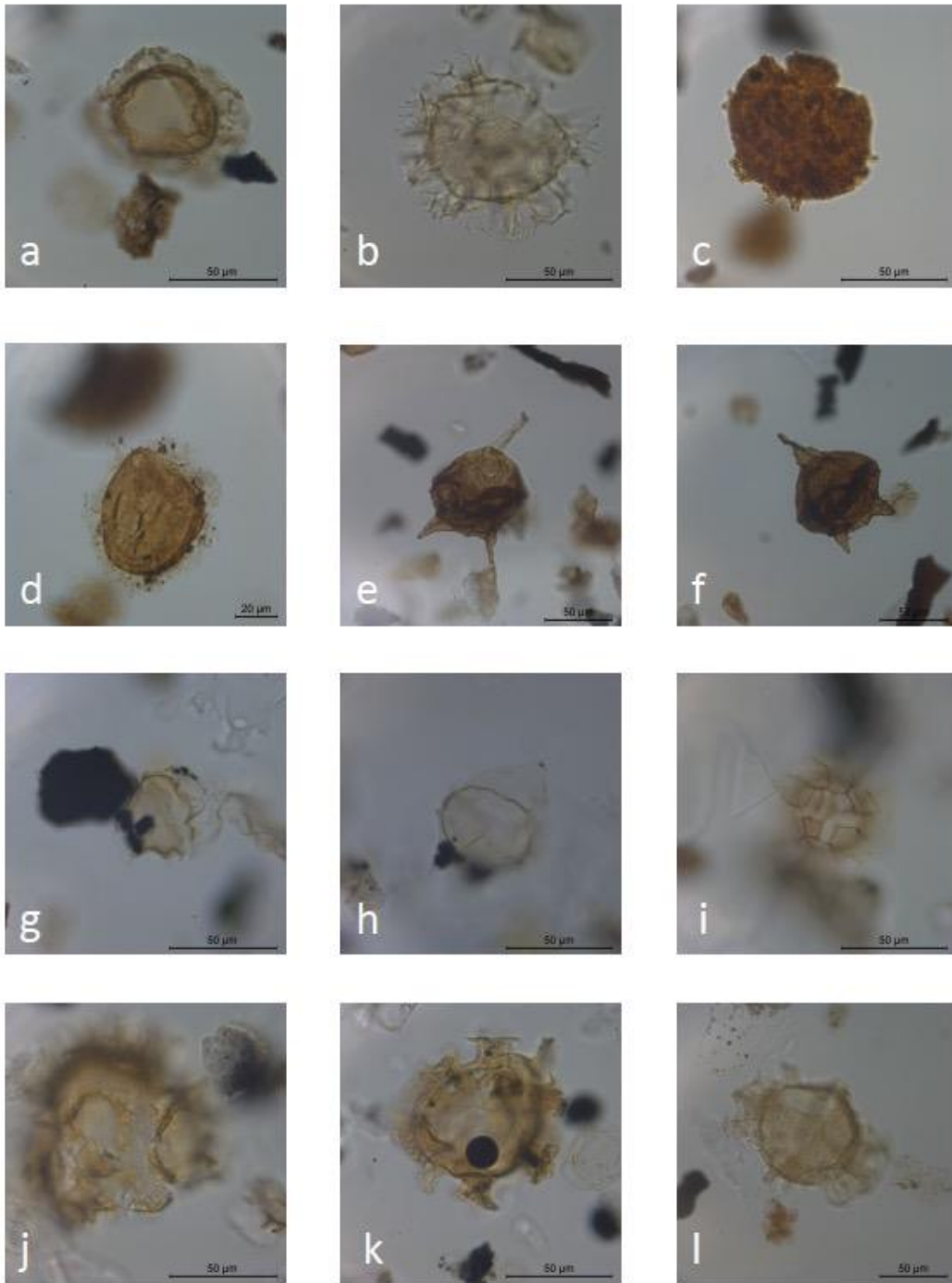
**Plate 2.** a: *Areoligera 'horrida'* 8601ft b: *Areoligera* spp. NSP 13 8608.0ft c: *Batiacasphaera* spp. NSP1 8727.5ft d: *Caligodinium aceras* NSP3 8586ft e: *Cerodinium speciosum* NSP15 8665.4ft f: *Cerodinium striatum* NSP3 8586ft g, h: *Chatagiella* sp. BRP37 1255.95ft i: *Cleistosphaeridinium placacantum* BRP9 1235.25ft j: *Cleistosphaeridinium* sp. BRP38 1257.15ft k, l: *Cordorsphaeridinium fibrospinsum* 8569.5ft, BRP14 1238.95ft
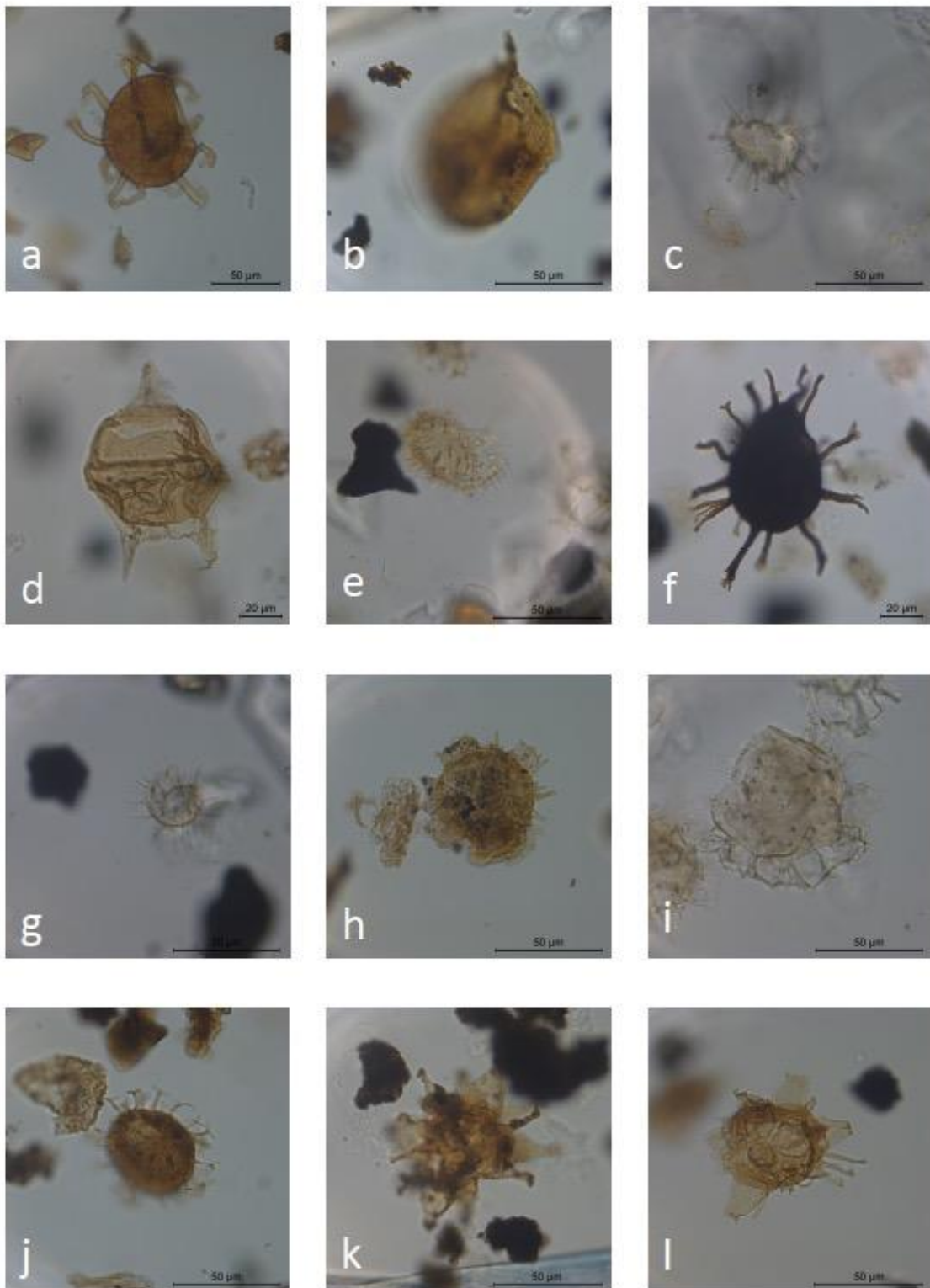
**Plate 3.** a: *Cordosphaeridinium gracile* NSP4 8617ft b: *Cribroperidinium* sp. NSP 11 8575.4ft c: *Dapsilidinium pastielsii* BRP32 1250.5ft d: *Deflandrea* sp. 8601ft e: *Eocladopyxis* sp. BRP33 1250.85ft f: *Fibrocysta vectense* 8550.5ft g: *Florentinia rechartii* BRP15 1239.65ft h: *Florentinia ferox* NSP14 8643.0ft i: *Glaphyrocysta ordinata* BRP6 1233.25ft j: *Hafniasphaera spetata*. NSP4 8617ft k, l: *Hystrichokolpoma bulbosum* NSP23 8867.7ft,
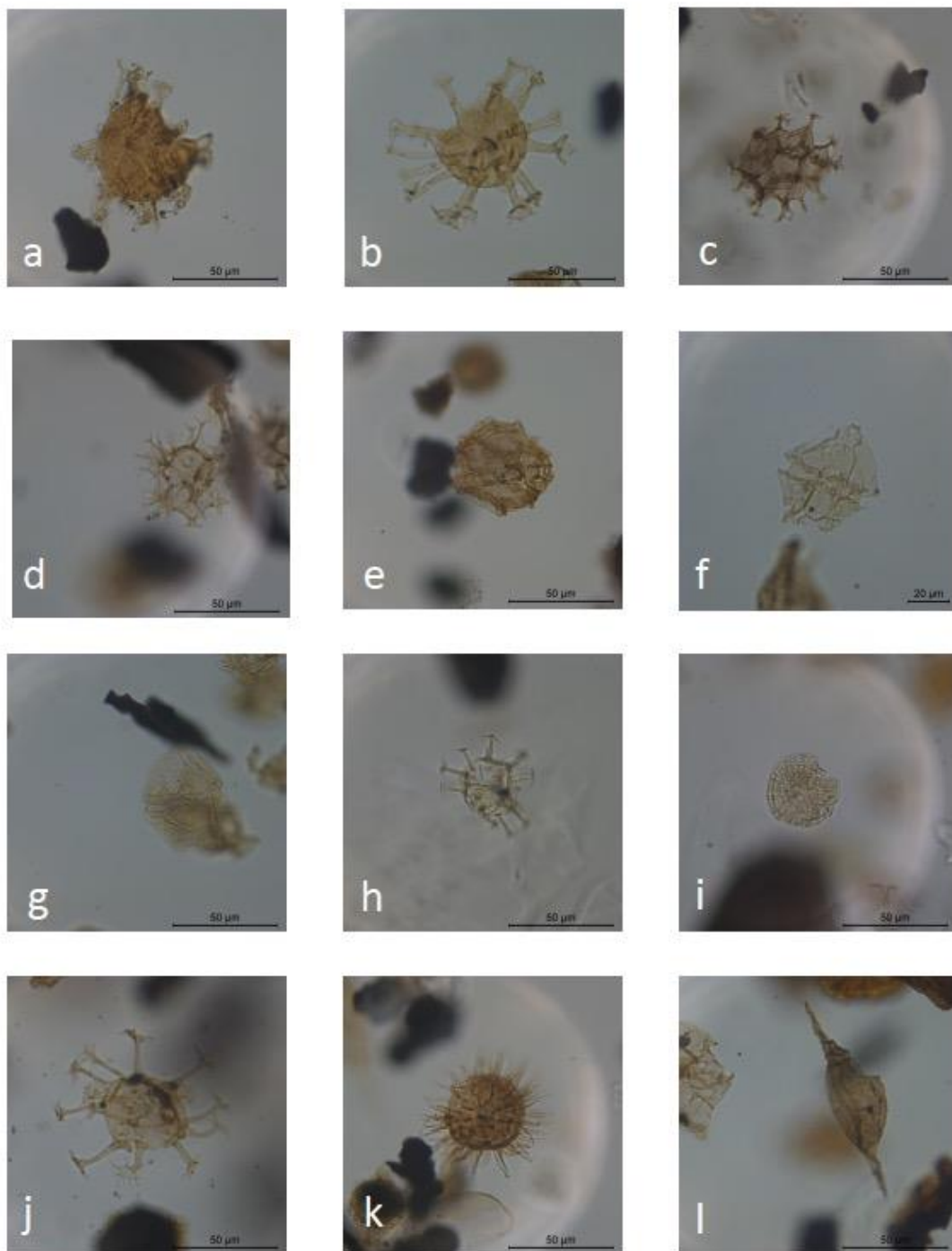
**Plate 4.** a: *Hystrichokolpoma truncatum* BRP28 1247.75ft b: *Hystrichosphaeridinium* sp. NSP4 8617ft c: *Hystristogylon coninckii* NSP15 8665.4ft d: *Hystristogylon membraniphora* NSP2 8559ft e: *Impagidinium* sp. NSP9 8508.8ft f, g: *Isabelidinium viborgense* 8601.0ft h: *Meltasphaeridinium* sp. BRP9 1235.25ft i: *Membranosphaera* spp. BRP11 1236.55ft j: *Oligoshaeridinium* sp.NSP6 8736.25ft k: *Operculodinium centrocarpum* 8772ft l: *Palaeocystodinium golzowense* 8653.4ft,
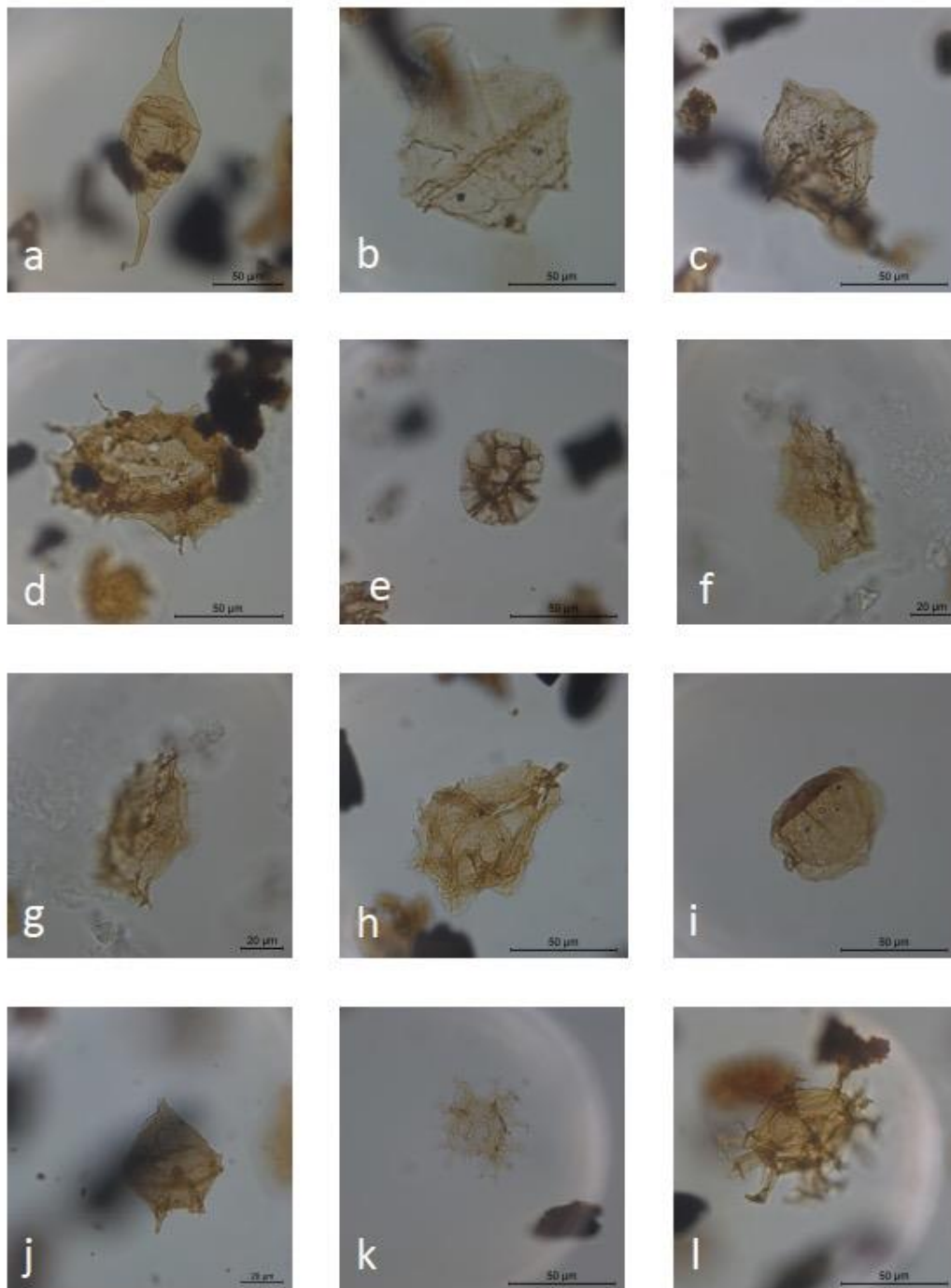
**Plate 5.** a: *Palaeocystodinium lidae* NSP14 8643ft b, c: *Palaeoperidinium pyrophorum* NSP3 8586ft d: *Palynodinium grallaror* NSP6 8847.05ft e: *Pancisphaeridinium* sp. NSP17 8723.8ft f, g: *Rottnestia borussica* NSP 23 8867.7ft h: *Senegalinium* spp. 8569.5ft i: *Senoniasphaera inornata* NSP20 8765.3ft j: *Spinidinium* sp. 8772ft k: *Spiniferites mirabilis* NSP14 8643ft l: *Spiniferites pseudofurcatus* NSP14 8643ft
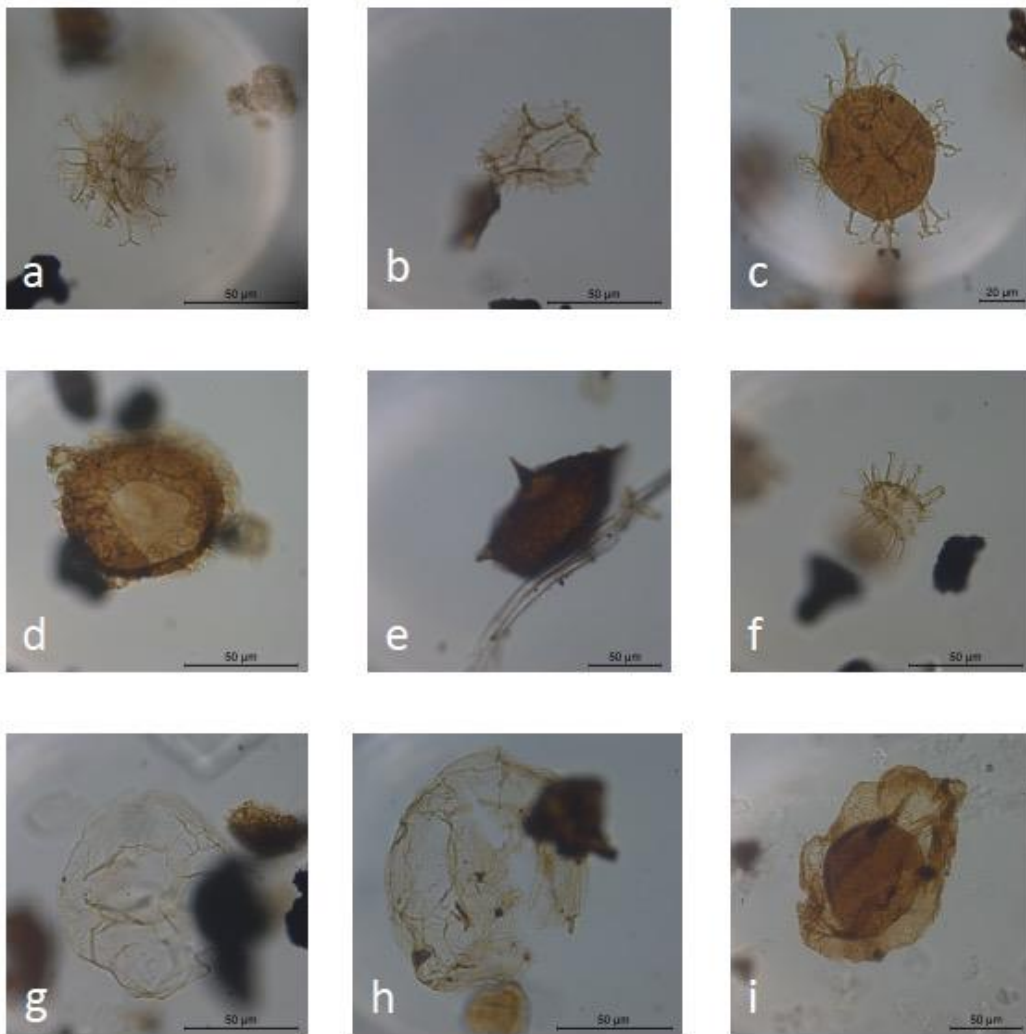
**Plate 6.** a: *Spiniferites ramosus* NSP18 8741.5ft b: *Spiniferites* spp. NSP4 8617ft c: *Spiniferella cornuta* 8653.4ft d, e: *Spongodinium* NSP8 8847.05ft f: *Tanyosphaeridinium* sp. NSP16 8687.5ft g, h: *Thalassphora delicata* 8601.0ft i: *Thalassphora pelagica* 8569.5ft
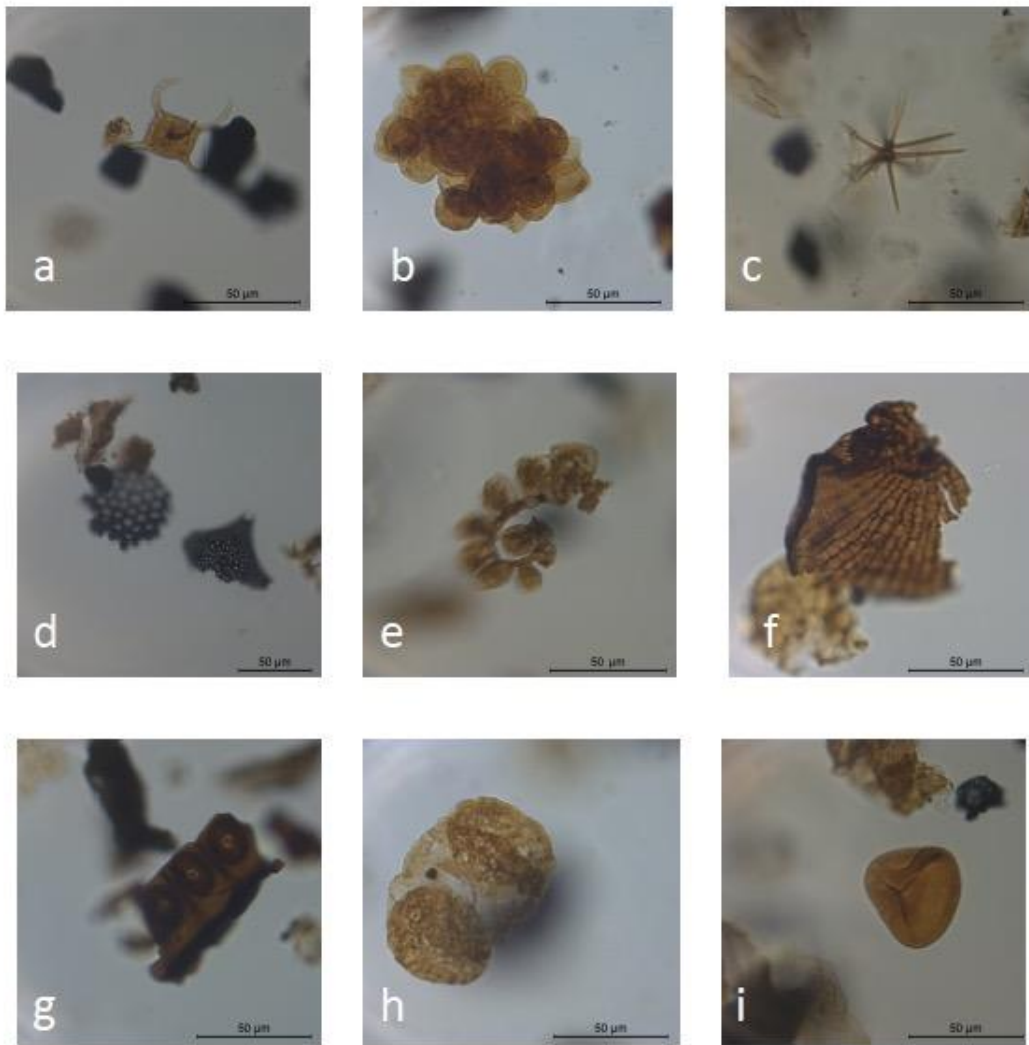
**Plate 7.** a: Acritarch NSP18 8741.5ft b: Acritarch NSP4 8617ft c: Acritarch sponge spikes 8653.4ft d: pyritized diatom e: foram lining NSP16 8687.5ft f: plant cuticula 8601.0ft g: plant stoma 8569.5ft h: bisaccate pollen i: trilete spore